iScience

CellPress

Article

Prostate Stroma Increases the Viability and Maintains the Branching Phenotype of Human Prostate Organoids

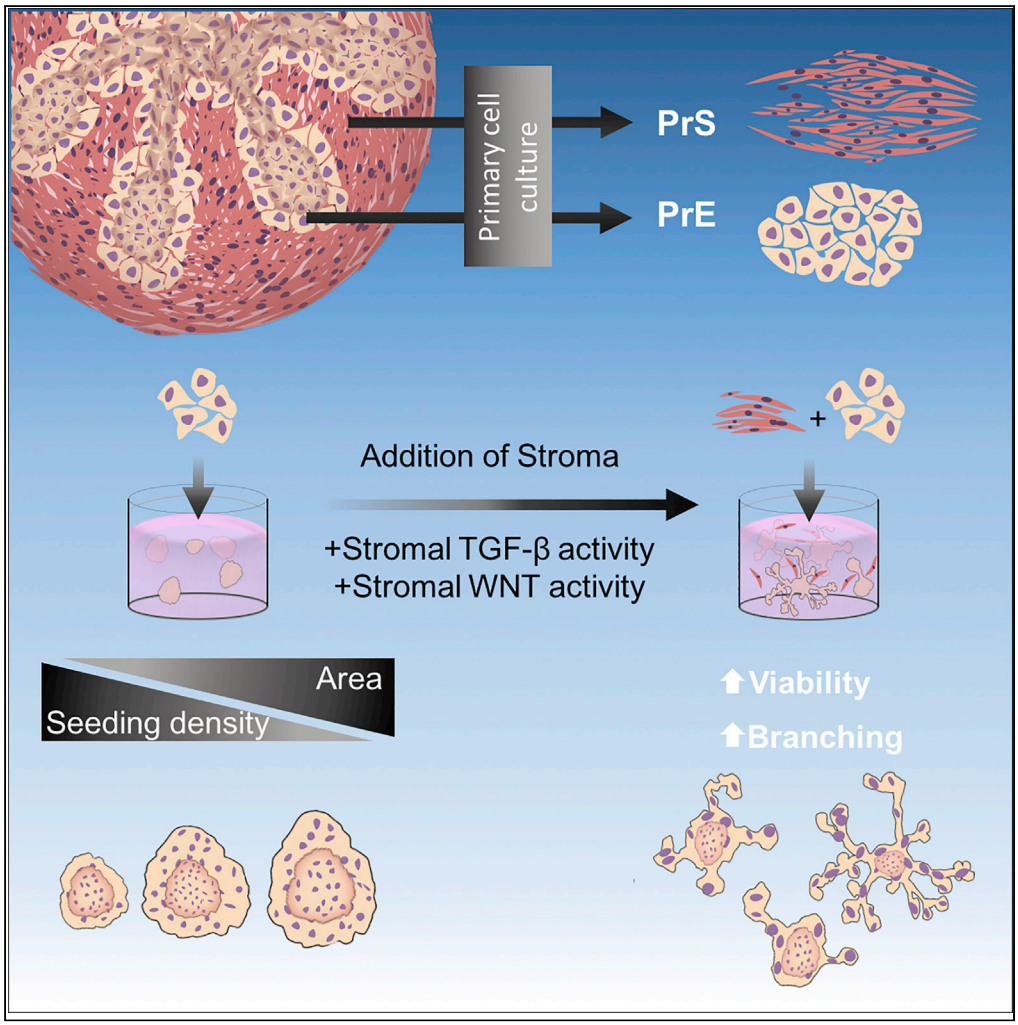

Zachary Richards, Tara McCray, Joseph Marsili, ..., Sarki A. Abdulkadir, Gail S. Prins, Larisa Nonn

lnonn@uic.edu

HIGHLIGHTS

Co-culture with human primary prostate stroma improves epithelial organoid viability

Stromal cell contact in co-culture directs epithelial organoid branching

Prostate stromal cells express morphogenic factors unique from non-prostate fibroblasts

Co-culture with stroma maintains AMACR and increases survival of cancer derived-organoids

Richards et al., iScience *12*, 304–317
February 22, 2019
https://doi.org/10.1016/j.isci.2019.01.028

iScience

CellPress

Article

Prostate Stroma Increases the Viability and Maintains the Branching Phenotype of Human Prostate Organoids

Zachary Richards,[1,7] Tara McCray,[1,7] Joseph Marsili,[1,2] Morgan L. Zenner,[1] Jacob T. Manlucu,[2] Jason Garcia,[1] Andre Kajdacsy-Balla,[1,6] Marcus Murray,[3] Cindy Voisine,[2] Adam B. Murphy,[4] Sarki A. Abdulkadir,[4] Gail S. Prins,[1,5,6] and Larisa Nonn[1,6,8,*]

SUMMARY

The fibromuscular stroma of the prostate regulates normal epithelial differentiation and contributes to carcinogenesis *in vivo*. We developed and characterized a human 3D prostate organoid co-culture model that incorporates prostate stroma. Primary prostate stromal cells increased organoid formation and directed organoid morphology into a branched acini structure similar to what is observed *in vivo*. Organoid branching occurred distal to physical contact with stromal cells, demonstrating non-random branching. Stroma-induced phenotypes were similar in all patients examined, yet they maintained inter-patient heterogeneity in the degree of response. Stromal cells expressed growth factors involved in epithelial differentiation, which was not observed in non-prostatic fibroblasts. Organoids derived from areas of prostate cancer maintained differential expression of alpha-methyl-acyl-CoA racemase and showed increased viability and passaging when co-cultured with stroma. The addition of stroma to epithelial cells *in vitro* improves the ability of organoids to recapitulate features of the tissue and enhances the viability of organoids.

INTRODUCTION

Prostate development and disease is primarily studied *in vitro* using a small set of immortalized or transformed benign and cancer cell lines. To more accurately study patient phenotypes and heterogeneity, primary cells are an alternative strategy but are limited in the number of passages and bias toward cells capable of growing on plastic. To address these concerns, three-dimensional (3D) organoid culture systems have been developed for *in vitro* use as an alternative to immortalized cell lines and animal models. Organoids reflect tissue structure and function while maintaining genetic diversity and lineage specificity (Wang et al., 2017). Single epithelial cells or cell aggregates from colon, breast, prostate, lung, pancreas, and salivary ducts cultured in 3D matrices can form fully differentiated organoids comprising cell types that closely mimic the structure and function of the *in vivo* tissue (Kretzschmar and Clevers, 2016).

Bipotent adult human and murine prostate progenitor cells of basal or luminal epithelial origin can differentiate into organoids with pseudostratified epithelium consisting of an outer layer of Ck5+ and p63+ basal cells, a single inner layer of Ck8/18+ and androgen receptor (AR)-expressing luminal cells, and central lumen closely resembling the *in vivo* acinar structure (Chua et al., 2014; Garraway et al., 2010; Karthaus et al., 2014). Although these current organoid models have improved modeling of differentiated tissues, they are limited because they lack incorporation of other cell types of the prostate gland, including neuroendocrine, immune, endothelial, and stromal cells.

The dominant cell type surrounding prostate epithelial (PrE) acini is a fibromuscular mesenchyme, also known as stroma, which exerts regulatory control over normal glandular differentiation and contributes to carcinogenesis (Niu and Xia, 2009). The stroma comprises the bulk of the prostate and contains fibroblasts, myofibroblasts, and smooth muscle cells (Farnsworth, 1999). The prostate mesenchyme influences gland formation during neonatal development, and stromal AR signaling is essential for normal gland morphogenesis (Cunha and Chung, 1981). Paracrine signaling between stroma and epithelium, which includes secreted WNTs, fibroblast growth factors (FGFs), sonic hedgehog, bone morphogenetic proteins (BMPs), and transforming growth factor (TGF) β, has positive and negative regulatory roles in adult PrE maintenance, regeneration, and transformation (Prins and Putz, 2008). Stroma-epithelial cross talk is

[1]Department of Pathology, University of Illinois at Chicago, 840 S Wood St., Chicago, IL 60612, USA

[2]Department of Biology, Northeastern Illinois University, Chicago, IL 60625, USA

[3]Project Brotherhood, Chicago, IL 60637, USA

[4]Department of Urology, Northwestern University Feinberg School of Medicine, Chicago, IL 60611, USA

[5]Departments of Urology, Physiology, and Biophysics, University of Illinois at Chicago, Chicago, IL 60612, USA

[6]University of Illinois Cancer Center, Chicago, IL 60612, USA

[7]These authors contributed equally

[8]Lead Contact

*Correspondence: lnonn@uic.edu

https://doi.org/10.1016/j.isci.2019.01.028

altered during prostate carcinogenesis wherein cancer-associated fibroblasts of the surrounding stroma trigger remodeling of the tumor microenvironment, which promotes prostate carcinogenesis and increases metastases (Barron and Rowley, 2012; Franco et al., 2010). Tissue recombination models of cancer-associated fibroblasts with PrE cells indicate that stromal alterations can induce epithelial transformation (Franco et al., 2011) and promote gland-forming capabilities of cancer stem cells (Liao et al., 2010). Furthermore, *in vitro* studies using stromal cells grown on a Transwell insert reveal that stromal secretions are essential for proper prostate organoid development and morphology (Lang et al., 2001) and response to hormones (Giangreco et al., 2015).

Culture conditions influence the phenotype of prostate organoids, and stromal regulation over epithelial cells is essential, yet a 3D model that includes prostate stroma has not been reported. To address this need, we systematically optimized and characterized a 3D co-culture model that facilitates direct stroma-epithelial organoid interaction. Under optimal co-culture conditions, the addition of prostate stroma to 3D organoid culture increases organoid formation efficiency, influences branching morphogenesis, demonstrates stromal-epithelial cross talk, and provides a model to recapitulate some of the *in vivo* phenotypes.

RESULTS

Addition of Human Primary Prostate Stromal Cells to 3D Culture of Human Benign Prostate Epithelial Cells Increases Organoid Branching

The method for co-culture using primary PrE and stromal cells was optimized by systematic modifications of cell density, matrix composition, culture medium, and plating format (Matrigel base layer or low-attachment plates). All experiments used human primary PrE and primary prostate stromal (PrS) cells as previously described (Giangreco et al., 2013; Nonn et al., 2006) at seeding densities from 1×10^3 to 2×10^4 cells/well in a 96-well microplate format. The PrS cells are composed of fibroblasts and smooth muscle cells, expressing *TIMP3*, smooth muscle actin (*SMA*), and vimentin (Figure 1A). Patient characteristics from which cells were derived are listed in Table 1. Matrigel compositions of 5% and 10% were tested in ultra-low-attachment microplates, and Matrigel compositions of 10%, 33%, and 50% were tested in flat-bottom microplates (data not shown). Co-cultures seeded in ultra-low-attachment microplates were undesirable; cells formed spherical aggregates rather than organoids derived from single progenitor cells (data not shown). The final optimal co-culture conditions consisted of a total cell density of 5×10^3 cells/well in 33% Matrigel, in a keratinocyte-serum-free medium base media with charcoal-stripped fetal bovine serum and dihydrotestosterone without ROCK inhibitor as determined by organoid number, growth, survival, and experimental endpoints.

The effect of stroma was first examined using PrE organoids and PrS cells derived from benign regions of radical prostatectomy tissue. The benign PrE cells from two patients were cultured using a 1:2 ratio of PrE:PrS (Figure 1B). Organoids, defined as multicellular acini-like structures derived from a single progenitor cell, were visible at day 7 in all cultures, and co-culture organoids exhibited a pronounced qualitative branching phenotype that mimicked normal acinar structure *in vivo*, whereas branching was rarely observed in mono-culture (Figure 1D). PrS cells were largely cytostatic in co-culture with $\sim 4 \times 10^3$ cells/well remaining after 7 days with few dividing cells observed through incorporation of a 5-Ethylnyl-2′-deoxyuridine (EdU)-Alexafluor647 analog (Figure 1C). To test if organoids form from single cells, PrE cells were independently labeled with GFP or red fluorescence protein (RFP), mixed, and seeded into 3D culture. None of the organoids co-expressed both RFP and GFP markers (Figure S1A). As well, daily imaging of PrE cells co-cultured with GFP-labeled PrS cells showed steady outgrowth rather than clumping, indicating that the organoids were of single progenitor cell origin (Figure S1B). Quantification and categorization of organoid branching according to a branching classification scheme confirmed that co-culture with stroma produced more branched organoids of more complex structures compared with mono-culture (Figure 1E). The branching phenotype was not unique to co-culture as branching was observed in mono-culture organoids in one of the patient tissues (PrE-2), but to a lesser extent than in co-culture (Figure 1E). In addition, time-lapse imaging for a period of ~24 h of day 7 organoids showed that branching morphogenesis is more complex and dynamic in co-culture (Video S1) compared with mono-culture (Video S2). Branching of a single organoid in co-culture shows morphogenesis over a 5-day period from days 6–10 (Figure 1F).

Organoids cultured in these co-culture conditions exhibited differentiation with mixed p63-positive and p63-negative cells (Figure 2A). Both mono and co-culture organoids formed lumens and contained AR+ and AR− cells demonstrating differentiation toward a luminal phenotype (Figures 2A, 2B, and S2A–S2C).

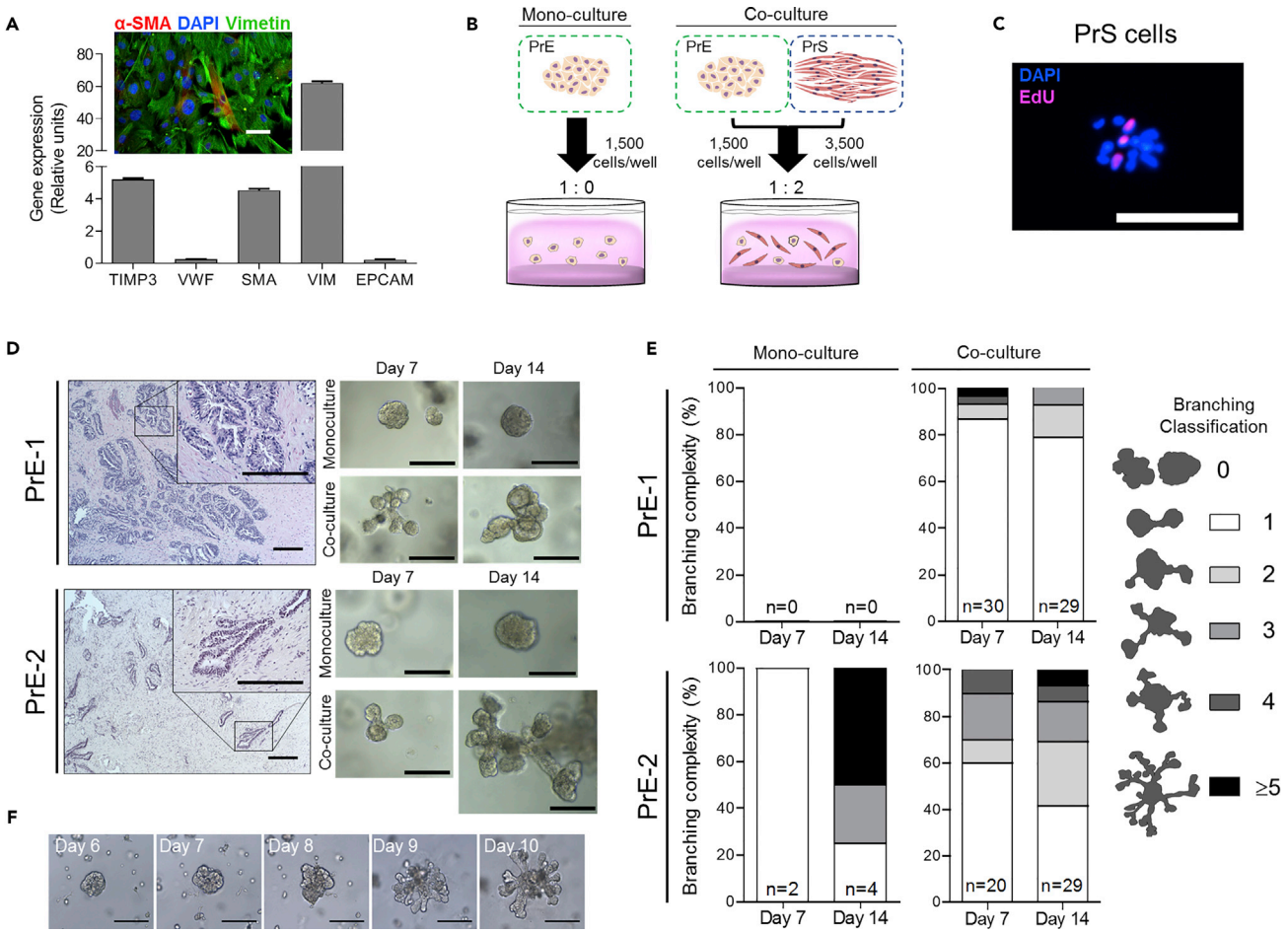

Figure 1. 3D Co-culture with Prostate Stroma Supports Organoid Growth and Increases Organoid Branching

(A) Gene expression of PrS mix 1 from microarray of stroma-specific genes *TIMP3*, von Willebrand factor (*VWF*), α-SMA (*ACT2* shown as SMA), and *EpCAM*. Quadruplicate measures reported; error bars represent one standard deviation of the mean. Stromal cells are a heterogeneous mixture of fibroblasts and myofibroblasts by immunofluorescent staining of α-SMA and vimentin in PrS mix 3. Scale bar, 100 μm.

(B) Schematic of mono-culture and co-culture workflow and conditions. PrE and PrS cells seeded into 33% Matrigel on top of 50% Matrigel base layer.

(C) Fluorescent images of PrS mix 1 incorporation of an EdU analog cultured in 3D conditions. Scale bar, 200 μm.

(D) Bright-field images of organoids in mono- and co-culture derived from dissociated epithelial cells isolated from benign prostate tissue specimens of two patients (PrE-1, top; PrE-2, bottom). Hematoxylin and eosin staining showing histopathology of patient tissue. Scale bar, 200 μm.

(E) Percentage of branched organoids in mono- and co-cultures on days 7 and 14 according to a branching classification scheme used to categorize each organoid by extent of branching (right). Quantification of organoid branching in mono- and co-cultures according to the branching classification scheme in organoids derived from two patients (PrE-1, top; PrE-2, bottom). Triplicate wells per condition, n reported as sum of branched organoids from triplicate wells per condition.

(F) Bright-field images of time course showing PrE-1 organoid branching from days 6–10 in co-culture with PrS mix 4. Scale bar, 200 μm.

However, the media was negative for prostate specific antigen (PSA) secretion by ELISA (data not shown) suggesting incomplete luminal differentiation. Organoids in co-culture had complex branches that expressed the basal marker Ck5 on the periphery and Ck8 throughout the organoid as visualized by whole-mount immunofluorescent imaging (Figure 2C and D) indicating that the organoid body was composed of epithelial cells. Unbranched organoids predominantly formed lumens (Figure S2A), and branched organoids had mixed morphology with solid and hollow branching structures (Figures S2B and S2C). For organoid co-culture, PrE cells from 12 patient tissues and one immortalized cell line (benign RWPE-1) were attempted with varying viability (Table 1). Tissues that generated viable organoids exhibited patient-specific heterogeneity in the extent of stroma-induced branching, and only one exhibited branching in the absence of stroma (Figure S3). Notably, cells that grew poorly as organoids in monoculture had increased viability when grown in co-culture with stromal cells (Figure S3, PrE-6 and PrE-7).

Primary Prostate Epithelial Cells					
Cell ID	Pathology of Tissue Region	Age (Years)	Race	Shown in Figure	Organoid Growth
PrE-1	Benign	71	AA	Figures 1, 2, 3, 4, and S1–S5	++++
PrE-2	Benign	68	AA	Figures 1, 3, S1, S4, and S5	++++
PrE-3	Benign	58	AA	Figures 5, S4, and S5	++
PrECa-3	Cancer 3 + 4			Figures 5 and S4–S6	+++
PrE-4	Benign	U	AA	Figures 5, S4, and S5	++
PrECa-4	Cancer 4 + 4			Figures 5 and S4–S6	++
PrE-5	Benign	60	AA	Figures 5 and S4	+++
PrECa-5	Cancer 3 + 3			Figures 5, S4, and S6	++++
PrE-6	Benign	57	EA	Figures S4 and S5	–
PrECa-6	Cancer 4 + 4			Figures S4–S6	+
PrE-7	Benign	62	EA	Figures S4 and S5	–
PrECa-7	Cancer 3 + 4			Figures S4–S6	++

Primary Prostate Stromal Cells				
Cell ID	Pathology of Tissue Region	Age	Race	Used in PrS Mix #
PrS-1	Benign	71	AA	3
PrS-3	Benign	58	AA	
PrS-8	Benign	64	AA	1, 2, 3
PrS-9	Benign	60	C	1, 2, 3
PrS-10	Benign	50	AA	1, 2
PrS-11	Benign	55	AA	1
PrS-12	Benign	71	AA	1
PrS-13	Benign	61	H	2, 5, 6
PrS-14	Benign	54	U	2
PrS-15	Benign	63	AA	4
PrS-16	Benign	61	AA	4
PrS-17	Benign	73	C	4
PrS-18	Benign	59	AA	4
PrS-19	Benign	66	AA	6
PrS-20	Benign	62	U	5, 6

Table 1. Human Primary Cell Patient Characteristics

PrS, primary stromal; PrE, primary epithelial; AA, African American; EA, European American; H, Hispanic; U, unavailable data.

Decreasing the Epithelial-to-Stromal Cell Ratio Increases Organoid Formation Efficiency and Decreasing Epithelial Seeding Density Alone Increases Organoid Size

Initial co-culture conditions demonstrated increased organoid branching by the addition of stroma. PrS cells from two patients (PrS-2, PrS-6) were used for initial studies shown in Figure 1. However, to provide continuity in the stromal source for subsequent experiments, PrS cells from 13 patients were mixed to

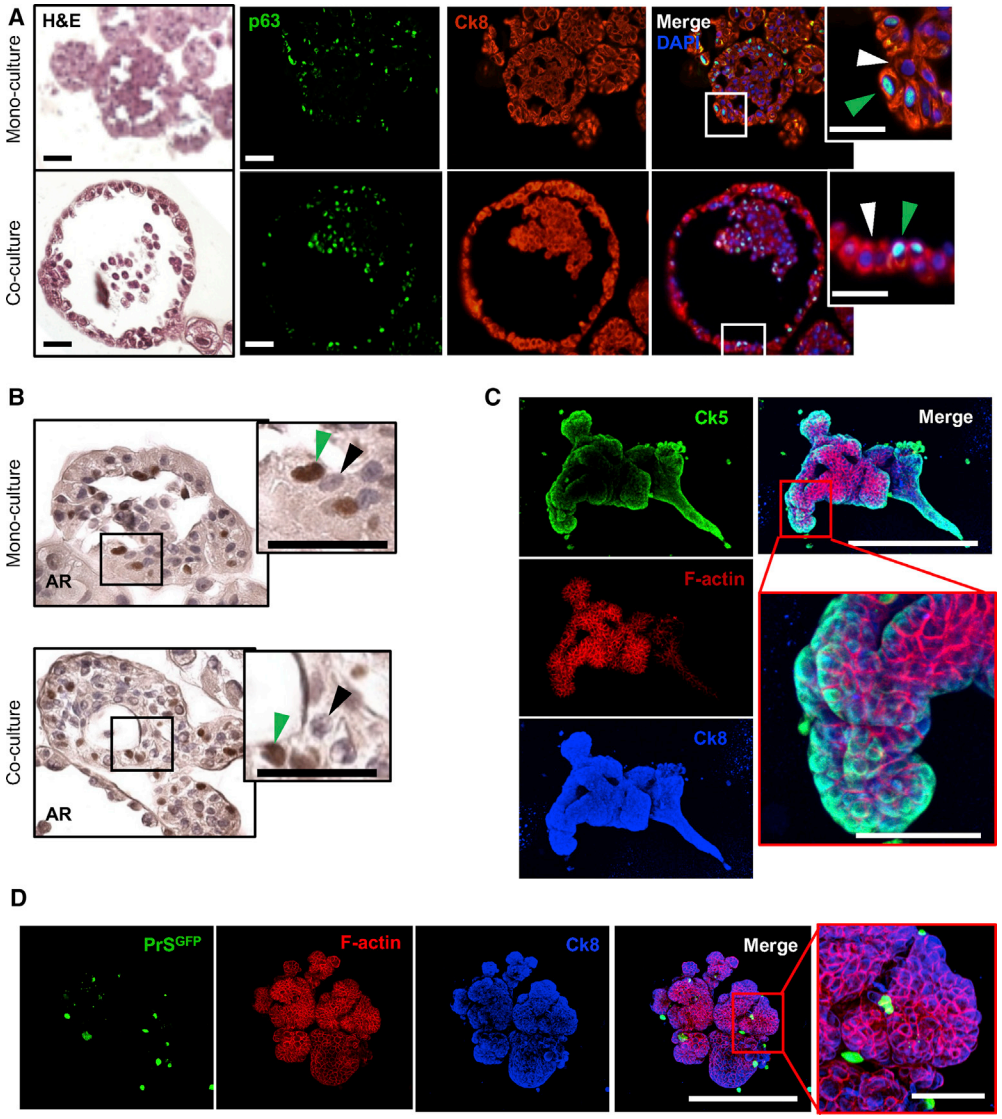

Figure 2. Organoids in Mono-culture and Co-culture Form Mixed Epithelial Differentiation and Contain Lumens

(A) H&E and immunofluorescent images of differentiation markers p63 and Ck8 of PrE-1 organoids in mono-culture and co-culture with PrS mix 1. Inset shows Ck8+ cells co-expressing p63 (green arrow) or p63− (white arrow). Scale bars, 50 μm.

(B) Immunohistochemical stain for AR in PrE-1 organoids in mono-culture and co-culture with PrS mix 1. Insets show high magnification of adjacent AR+ (green arrow) and AR− (black arrow) cells. Scale bars, 50 μm.

(C) Whole-mount immunofluorescent staining of Ck5 (green), Ck8 (blue), and phalloidin (red) in day 14 PrE-2 organoids co-cultured with PrS mix 1. Scale bars, 500 μm (merge) and 100 μm (zoom).

(D) Whole-mount immunofluorescent staining of organoid with PrS-GFP cells (green), Ck8 (blue), and phalloidin (red) in day 12 PrE-1 organoids cultured with GFP-labeled PrS mix 3. Scale bars, 500 μm (merge) and 100 μm (zoom).

form a total of 6 pools, cryopreserved at low passage, and thawed for each experiment (Table 1). Notably, co-culture with PrS-2, PrS-6, or PrS pools stimulated organoid branching, indicating that stromal induction of branching was not unique to one stromal line. This phenotype was further assessed through alteration of the ratio of stromal to epithelial cells in the co-culture by examining various PrE:PrS seeding ratios. The total number of cells per well was kept constant at 5×10^3, and ratios of 1:1, 1:2, and 1:4 (PrE:PrS) were used. To ensure accurate unbiased quantification of organoids, an imaging and analysis pipeline was created to quantify organoid number and size in 3D culture. Whole-well images were captured at 25 z-planes encompassing the entire 3D matrix and compressed to generate a single enhanced depth-of-field, in-focus image

of each well for analysis (Figure 3A). This imaging method enabled quantification of each organoid *in situ* at multiple time points without disturbance of the culture. Resultant image analysis revealed that organoid formation efficiency, quantified on day 7, was significantly higher in co-cultures at PrE:PrS ratios of 1:2 ($p < 0.05$) and 1:4 ($p < 0.0001$) compared with mono-culture controls that contained an equal number of PrE cells but lacked stroma (Figure 3B). In addition, there was a significant positive linear trend for organoid formation efficiency in the co-cultures as the PrE:PrS ratio decreased ($p < 0.0001$); this trend was absent in mono-culture (Figure 3B).

Organoid size was assessed on day 14 by quantifying the area of each organoid using the whole-well images generated from the imaging pipeline. Organoids in co-culture had significantly smaller areas in the 1:1 PrE:PrS conditions, but no difference in organoid size between mono- and co-cultures was observed at the lower PrE:PrS ratios of 1:2 or 1:4 (Figure 3C). There was also a significant positive linear trend by ANOVA for organoid area in the mono-cultures as PrE seeding density decreased ($p < 0.0001$) (Figure 3C). Although co-culture with stroma significantly increased organoid formation efficiency, organoid size appeared to be a consequence of PrE seeding density alone, and variation of PrE to PrS ratio had no effect on area.

Addition of Stromal Cells to Co-culture Alters Organoid Morphologies

The combined effect of adding stroma to the co-culture and altering the PrE seeding density was further dissected to determine which was responsible for the observed phenotypes. Reduction in PrE seeding density to 250, 100, or 50 cells/well in co-culture with 5×10^3 PrS cells preserved the branching phenotype and enhanced organoid size; indeed, organoids seeded at these very low densities grew to >1 mm in diameter and were visible with the naked eye (Figure 3D). To validate the observed increase in formation efficiency as a consequence of co-culture with stroma, increasing quantities of stroma (1×10^3, 5×10^3, or 1×10^4 PrS/well) were co-cultured with PrE cells seeded at 100 cells/well for final PrE:PrS ratios of 1:10, 1:50, and 1:100. Addition of stroma significantly increased organoid formation efficiency, consistent with results at higher PrE densities, but no "dose effect" was observed, as organoid formation efficiency plateaued at ~50% regardless of stromal quantity (Figure 3E). Organoid area was also unaffected by the addition of stroma in these low-PrE-density culture conditions and consistent with results at higher PrE densities (Figure 3F).

To objectively quantify organoid branching morphology in an automated manner, measurements of area, circularity, and maximum/minimum radius ratio were used as indicators of structure complexity (Figure 3A). Circularity was calculated as the ratio of the area of an organoid against a circle whose diameter is equal to the organoid's maximum Feret diameter and provides a value of 0–1, where 1 corresponds to a perfect circle and values < 1 indicate a more complex structure. Calculation of the maximum/minimum radius ratio enabled quantification of organoid structure, where a value of 1 indicated no branching and a value >1 corresponded to the magnitude of the largest branch from the center of the object. Organoids grown in co-culture had significantly greater area on day 7 compared with mono-culture organoids, but this effect was absent by day 14 (Figure 3G). Organoids in co-culture were significantly less circular and had significantly greater maximum/minimum radius ratios compared with those in mono-culture on days 7 and 14, consistent with a more branched phenotype (Figure 3G). Furthermore, quantification of area and circularity revealed that although mono- and co-culture organoids were similarly sized, their circularities could differ considerably (Figure 3G, mono: blue circle, co: red square). Analysis and quantification of organoid structure using our imaging pipeline provided a complete and robust assessment of branching morphologies and revealed several structural differences due to the addition of stroma.

Prostate Stromal Cells Influence Organoid Branching Morphogenesis via Cell-Cell Contact and Express Factors that Regulate Branching

The branching process of organoids was observed by time-lapse video of single organoids and demonstrated stromal cell taxis and pseudopodia extension toward an organoid (Video S3). Direct stromal-organoid cell contact also appeared to influence organoid budding, branching, and stalk elongation: bud formation and branch extension occurred upon, or immediately before, stroma-organoid interaction (Figure 4A, black arrowheads) (Video S4). In each observed occurrence, organoid budding and stalk elongation occurred distally to stromal cell contact (Figure 4A) (Videos S5 and S6). Branching appeared to arise as a stochastic process influenced by the presence of stroma, and rare instances of branch detachment

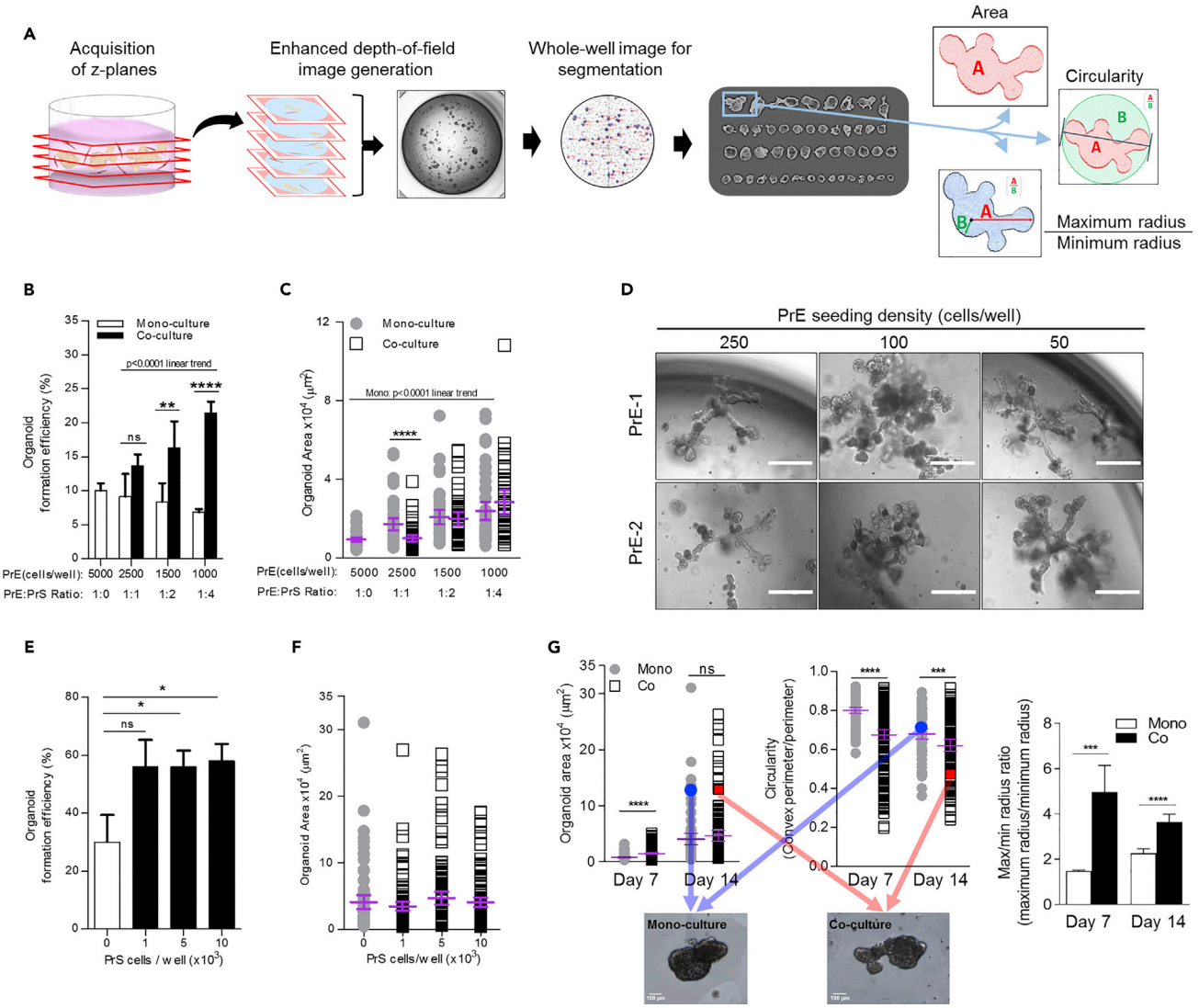

Figure 3. Differential Effects of the Epithelial-to-Stromal Cell Ratio and Epithelial Seeding Density on Organoid Formation Efficiency, Size, and Branching Morphologies

(A) Pipeline for whole-well imaging and analysis. Image acquisition at 25 z-planes per well, generation of a single enhanced depth-of-field image, conversion to grayscale, and identification of each organoid. The area, circularity, and maximum/minimum radius ratio were calculated for each organoid in every well. Calculation details can be found in Methods.

(B) Organoid formation efficiency percentage (number of organoids per number of PrE seeded) for mono and co-cultures. Triplicate wells per condition; errors bars represent one standard deviation of the mean.

(C) Area quantification of organoids in mono and co-cultures. Triplicate wells per conditions; error bars show mean with 95% confidence interval.

(D) Representative bright-field images depicting branching morphologies of organoids in co-culture derived from two patients, PrE-1 and PrE-2, at various PrE seeding densities. Scale bars, 500 µm.

(E) Organoid formation efficiency (number organoids per number of PrE cells seeded) in mono-culture (white bar) and co-culture (black bars) seeded at 100 PrE cells/well with increasing numbers of PrS cells. Triplicate wells per condition; error bars represent one standard deviation of the mean.

(F) Area quantification of organoids in mono-culture (gray circles) and co-culture (white squares) with increasing numbers of PrS cells. Each dot represents a single organoid; data from triplicate wells combined. Error bars show mean with 95% confidence interval.

(G) Quantification of organoid area (left), circularity (middle), and maximum/minimum radius ratio (right) at days 7 and 14. Enhanced depth-of-field images (bottom) of a single organoid in mono-culture and co-culture and their corresponding area and circularity metrics on the graphs above (Mono, blue circle; co, red square). Each data point represents a single organoid from triplicate wells. Error bars show mean with 95% confidence interval for area and circularity and standard error of the mean for maximum/minimum radius ratio. Scale bar, 100 µm.

All data from PrE-1 and PrS mix 2 except where noted. p value <0.1 was considered statistically significant. *p < 0.1, **p < 0.05, ***p < 0.01, ****p < 0.001; ns, not significant.

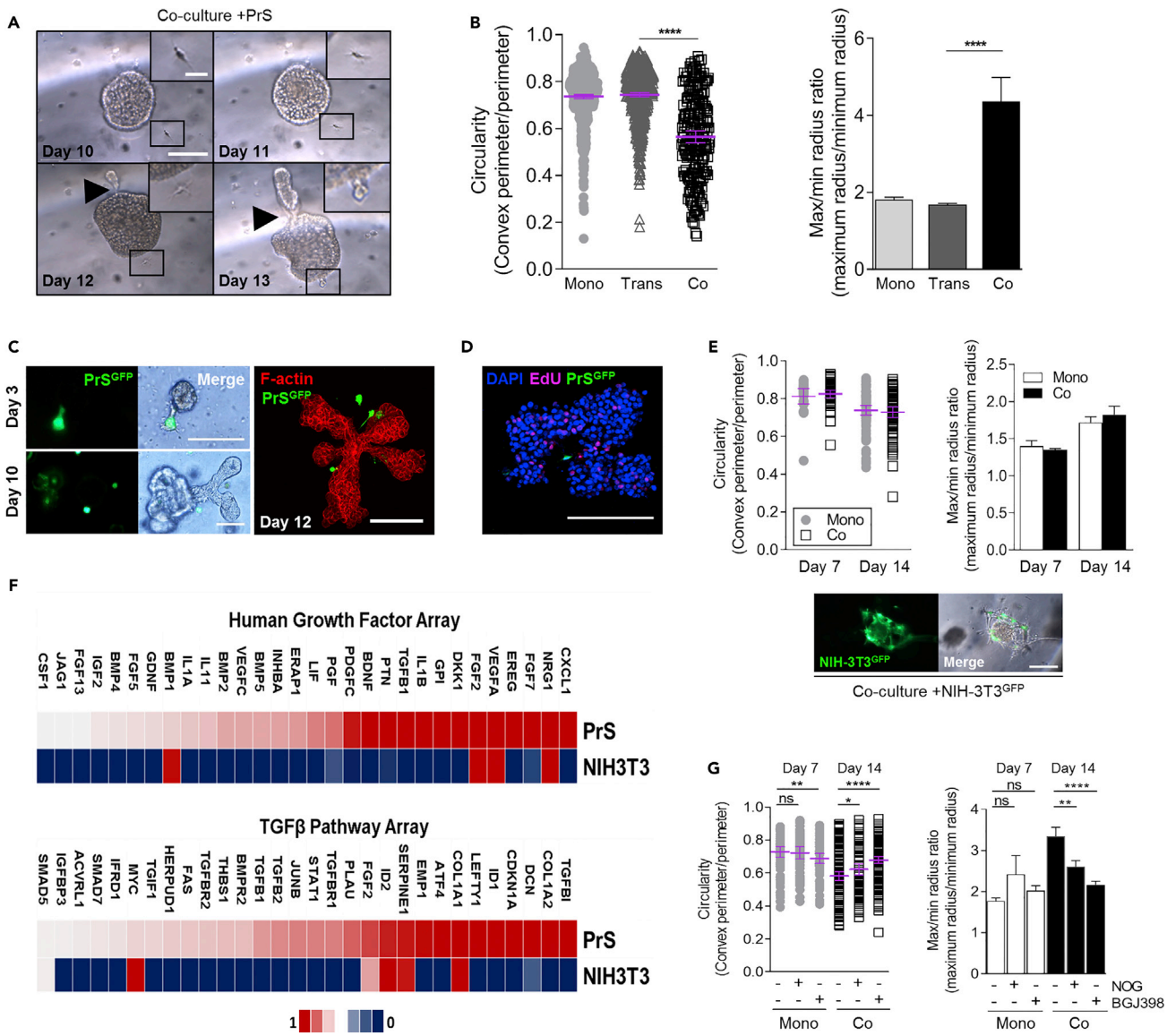

Figure 4. Stromal Cells Influence Organoid Branching Morphogenesis via Cell-Cell Contact and Express Unique Factors Compared with Non-prostate Fibroblasts

(A) Bright-field image on sequential days of stromal cell (boxed and zoom) taxis toward an organoid followed by distal bud formation (black arrow). Large scale bar, 200 μm; small scale bar, 50 μm. PrE-1 in co-culture with PrS-2.

(B) PrE-1 organoids grown in mono-culture (mono), Transwell co-culture (Trans), or direct co-culture (Co) with PrS mix 4 stromal cells. Circularity and maximum/minimum radius ratio measurements quantified from triplicate wells per condition; error bars show mean with 95% confidence interval for circularity and standard error of the mean for maximum/minimum radius ratio.

(C) Bright-field and fluorescent images of GFP-labeled PrS mix 3 cells in co-culture with PrE-1 organoids at days 3 and 10. Fluorescent images of GFP-labeled PrS mix 3 cells in co-culture with PrE-1 organoids at day 12 with phalloidin (red) in bottom panel. Scale bars, 200 μm.

(D) Fluorescent image of GFP-labeled PrS mix 3 cells in co-culture with PrE-1 epithelial organoid incorporation of an EdU analog (pink). Scale bar, 200 μm.

(E) Bright-field and fluorescent images of GFP-labeled NIH3T3 cells co-cultured with PrE-1 organoids. Circularity and maximum/minimum radius ratio measurements of organoids in mono-culture and co-culture with NIH3T3 cells. Triplicate wells per condition; error bars show mean with 95% confidence interval for circularity and standard error of the mean for maximum/minimum radius ratio. Scale bar, 200 μm.

(F) Comparative gene expression profiling of the human growth factors and TGF-β pathway by qPCR arrays in PrS mix 1 and NIH3T3 cells grown in 3D conditions. Array normalization details in Methods section.

(G) Circularity and maximum/minimum radius ratio measurements of organoids in mono-culture and co-culture treated with Noggin (NOG) or FGFR inhibitor (BGJ398). PrS mix 4 and PrE-1 organoids used in triplicate wells per condition; error bars show mean with 95% confidence interval for circularity and standard error of the mean for maximum/minimum radius ratio.

p value < 0.1 was considered statistically significant. *p < 0.1, **p < 0.05, ***p < 0.01, ****p < 0.001; ns, not significant.

were also observed (Video S7). Organoid branching required direct co-culture and contact with PrS as co-culture using a Transwell insert failed to significantly alter organoid circularity or maximum/minimum radius ratios (Figure 4B).

In addition to influencing branching through direct contact with organoids, GFP-labeled PrS cells associated around larger and more complex organoid structures (Figures 4C, S2A, and S2C) (Video S8), and with actively proliferating epithelial organoids indicated by incorporation of EdU (Figure 4D). PrS cells moved throughout the culture via contraction and expansion of pseudopodia as well as remodeling of the surrounding matrix (Video S9).

To test the specificity of prostate-derived stroma to mediate branching, co-culture with NIH3T3 cells was examined. Co-culture with GFP-labeled NIH3T3 embryonic mouse fibroblasts also resulted in extensive contact with organoids (Figure 4E) (Video S10), but did not increase organoid branching, as assessed by circularity and maximum/minimum radius ratios (Figure 4E). Similar to co-culture with PrS, addition of NIH3T3 cells significantly increased the organoid formation efficiency; however, in contrast, it also increased the organoid area on day 14, an effect not observed with PrS culture (Figures S4A and S4B). Overall, the branch induction of organoids was specific to PrS as the source of stroma, suggesting prostate-specific factors in morphogenic regulation.

The expression of morphogenesis-related genes in 3D PrS cells, with NIH3T3 fibroblasts for comparison, was quantified using qRT-PCR profiling arrays for TGF-β pathway and human growth factors. NIH3T3 cells expressed only 7 of the 20 genes most highly expressed by PrS cells in the TGF-β pathway and just 6 of the top 20 genes expressed by PrS cells in the Human Growth Factors array (Figure 4E). Notably, genes involved in the induction of prostate branching and gland development—FGF7, FGF2, LEFTY1, and DKK1—were highly expressed in PrS cells grown in 3D (Figure 4E). The mesenchymal secreted proteins BMP1, BMP4, BMP5, and FGF7 were highly expressed by the PrS cells and are known morphogenic factors in branching morphogenesis of the developing prostate (Prins and Putz, 2008). Addition of the BMP inhibitor Noggin, or the FGF receptor (FGFR) inhibitor BGJ398, significantly decreased organoid branching in the co-culture compared with mono-culture as assessed by circularity and maximum/minimum radius ratio measurements (Figure 4G). *TGF-ß1*, *TGF-ß2*, *TGF-ßI*, and *TGF-ßR2* were also highly expressed in the PrS cells; however, treatment with a TGF-β-neutralizing antibody had no effect on organoid branching in the co-culture (data not shown).

Co-culture Organoids Grown from Benign and Cancer Regions of the Same Patient Maintain Histologic Phenotype and Improve Passaging

Given the current challenges in the culture of organoids from localized prostate cancer, we tested if the addition of stroma would increase viability and maintain phenotypes observed in the tissue from which the cells were derived. Cells from five patient tissues were isolated from punches taken at a 100% cancer region (PrECa-3, PrECa-4, PrECa-5, PrECa-6, and PrECa-7) and a 100% benign region (PrE-3, PrE-4, PrE-5, PrE-6, and PrE-7), as confirmed by a board-certified pathologist (Figures 5A, 5B, and S3), and co-cultured with a cryopreserved PrS cell mixture to provide a consistent stromal source. AMACR (alpha-methylacyl-CoA racemase) is a well-established marker for prostate cancer (PCa) (Ananthanarayanan et al., 2005; Jiang et al., 2004; Rubin et al., 2002) and immunohistochemistry confirmed that the benign tissue from which the organoids were derived had low AMACR expression, whereas the matched cancer tissues had high AMACR expression (Figures 5A and 5B). Immunohistochemical staining and qRT-PCR of the organoids showed a similar pattern of AMACR expression, with the highest observed in the co-cultured organoids derived from the cancer areas (Figures 5C and S5, four patients shown). The organoids derived from these patients, both from benign and cancer, were notably smaller and less differentiated than other patients, which may be a result of patient heterogeneity.

To assess the ability of stroma to improve long-term viability of cancer-derived organoids, organoids derived from cancer regions of the four patients were passaged twice. Two of the mono-culture organoids did not survive passaging, whereas their co-culture counterparts thrived and maintained *AMACR* expression (Figures 5C and S5). Quantification of *AMACR* at the first and last passages showed that differential expression was maintained only in the presence of the stromal cells. Of note, organoids from Gleason 3 + 3 tumors grew better in general than those from higher grade (Table 1, Figures S3 and S6).

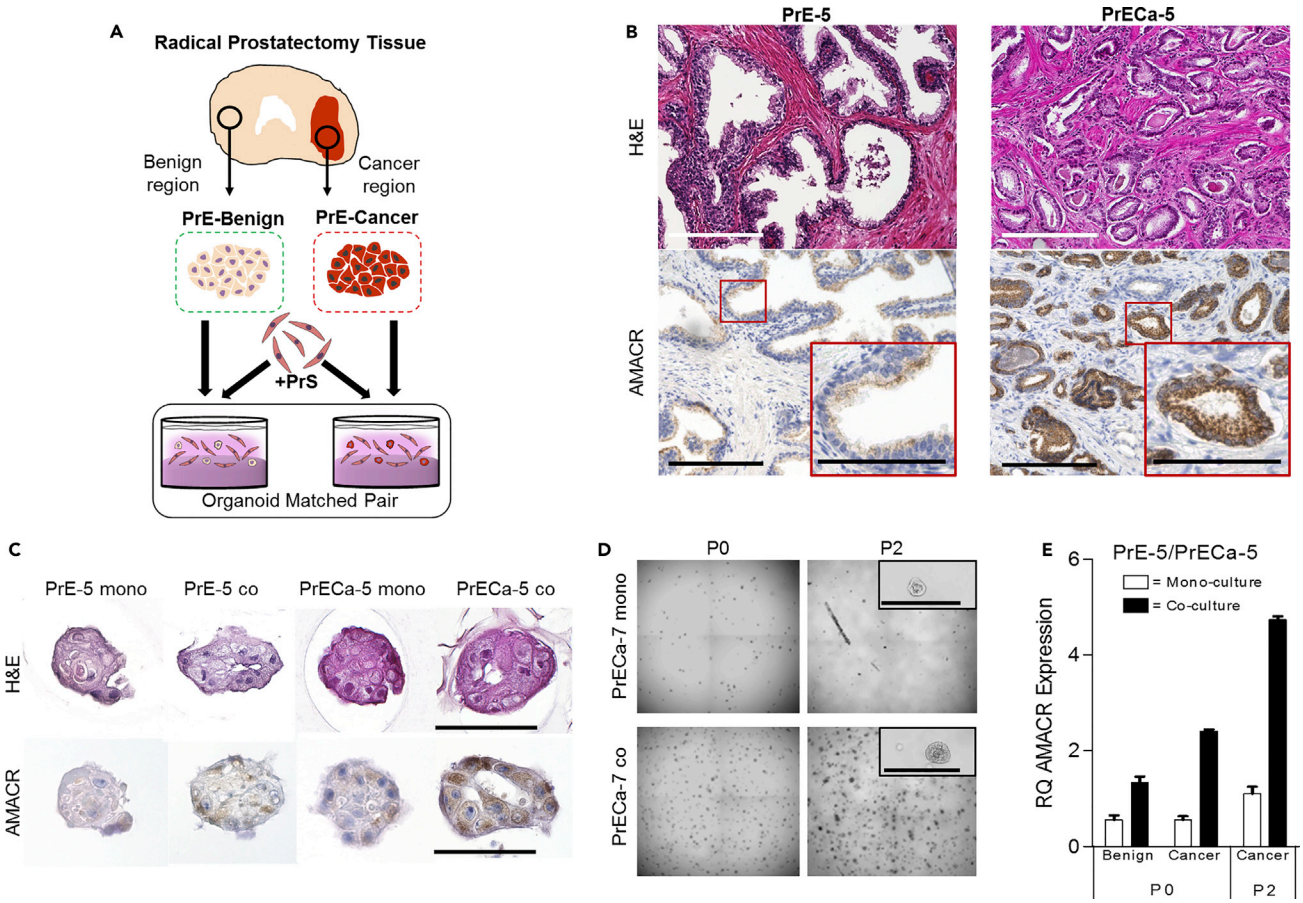

Figure 5. Co-culture Organoids Grown from Benign and Cancer Regions of the Same Patient Maintain Histologic Phenotype and Improve Passaging

(A) Isolation and co-culture of matched primary prostate organoids derived from benign and cancer regions of the same patient, with PrS cells.

(B) Matched benign (PrE-5) and cancer (PrECa-5) tissue from the patient from which cells were isolated for organoid growth. Histology shown by hematoxylin and eosin staining (top panel), and presence of AMACR shown by immunohistochemistry (bottom panel). 10X image shown with 40X inset for AMACR.

(C) Matched organoids derived from benign regions (PrE-5) and cancer regions (PrECa-5) from patient tissue shown in (B) grown in mono-culture and co-culture in 3D with PrS mix 5. Histology shown by hematoxylin and eosin staining (top panel), and presence of AMACR shown by immunohistochemistry (bottom panel). 40X images shown with 100-μM scale bar.

(D) Whole-well images of passage 0 and passage 2 mono- and co-culture PrECa-7 organoids derived from cancer regions. High magnification of selected organoid shown in inset. Inset shown with 100-μm scale bar.

(E) Expression of *AMACR* by qRT-PCR in total RNA isolated from matched organoids derived from benign and cancer tissue shown in (C) and passage 2 organoids shown in (D). Note that the benign organoids did not survive passage.

p value < 0.1 was considered statistically significant. *p < 0.1, **p < 0.05, ***p < 0.01, ****p < 0.001; ns, not significant.

DISCUSSION

The current *in vitro* 3D models of human PrE organoid lack the surrounding stroma. The influence of stroma on adjacent epithelium has been studied *in vivo* using xenografts (Sasaki et al., 2017) and *in vitro* using Transwell inserts (Lang et al., 2001; Giangreco et al., 2015), but this is the first study, to our knowledge, to enable direct prostate stroma-epithelium interaction in a 3D matrix and determine the paracrine role of stroma in human epithelial organoid growth and phenotype. We systematically optimized 3D co-culture conditions to combine both stroma and epithelial cells into the organoid model. Addition of human primary prostate stroma resulted in significant phenotypic effects on human PrE organoids.

Inclusion of stroma facilitated the striking phenotype of increased branching and morphologic complexity in co-cultured organoids. Budding and branching in the developing prostate gland is mediated by the surrounding urogenital mesenchyme and precedes glandular function (Hayward et al., 1997). Organoid

branching *in vitro* mimics the normal *in vivo* prostate acinar structure, thus providing an improved model of benign prostate. Branching rarely occurred in mono-culture, whereas the addition of stroma resulted in increased organoid branching that was visible subjectively and confirmed through objective quantification. In addition, the extent of branching varied by patient and highlights the *in vitro* preservation of inter-patient heterogeneity of primary prostate cells. This phenotype was not observed when non-prostate fibroblasts were used for co-culture, demonstrating that prostate stroma has unique regulatory control of the prostate epithelium. Organoids in both mono- and co-culture stained for markers indicating differentiation toward a luminal phenotype and expressed AR. However, PSA was not detected in the media and *KLK3* expression was minimal, indicating that stroma was not able to overcome this limitation in *in vitro* prostate organoid models.

Our imaging and analysis pipeline expedited quantitative morphological analysis of branching observations and overcame limits in current imaging modalities to quantify 3D objects in 3D space. In doing so, we deployed a simple solution to achieve whole-well imaging and enhanced depth-of-field image compression. Our imaging and analysis pipeline provided complete and robust organoid morphology metrics, even with the limitation of quantifying 3D objects from 2D images. We observed cell-cell interactions that were apparent through extensive still and time-lapse imaging. Others have shown that cell-matrix interactions also influence fibroblasts in 3D culture; for example, the presence of pure collagen promotes fibroblast dynamics (Åkerfelt et al., 2015). Our study explored variations in Matrigel densities; however, the use of additional or combined matrices such as collagen or synthetic gels may further enhance both organoid and stromal phenotypes and allow fine-tuning of optimal co-culture conditions (Gjorevski et al., 2016).

One advantage of direct co-culture over a Transwell insert is direct stroma-organoid contact. Comparison of Transwell versus direct co-culture methods demonstrated that stromal induction of organoid branching was unique to direct co-culture. An intriguing observation is that direct stromal contact appeared to promote organoid branching exclusively on the distal side, whereas branching appeared random in mono-culture. These findings in mono-culture support the work of Hannezo et al. who recently theorized that epithelial organoid branching is a stochastic and self-organizing process (Hannezo et al., 2017). In co-culture, branching is likely driven by several paracrine factors including FGFs, BMPs, and WNTs that have been reported to influence prostate epithelium development (Prins and Putz, 2008). BMPs and FGFs influenced organoid morphology in our co-culture condition as inhibition of BMPs (by Noggin) or FGFR significantly decreased organoid branching. Noggin was highly expressed in the PrS cells (Ct value = 29) compared with non-prostate fibroblasts, but addition of Noggin alone did not recapitulate the branching phenotype. Noggin is often included in organoid culture medium (Karthaus et al., 2014), yet branching is not observed in those models. This may be explained by the non-specific perturbation of Noggin spatial gradients, differing from the normally tightly regulated balance of inhibitory and stimulatory proteins observed during branching morphogenesis (Prins and Putz, 2008). The aforementioned paracrine factors, as well as other juxtacrine factors, also likely contribute to the branching phenotype and warrant further study.

TGF-β1 is highly expressed in mouse mesenchyme during epithelial duct formation (Prins and Putz, 2008) and has been previously reported to inhibit branching morphogenesis in mammary tissue and prostate tissue (Hannezo et al., 2017; Silberstein and Daniel, 1987; Prins and Putz, 2008). Analysis of the TGF-β pathway in stromal cells cultured in our prostate model revealed high expression of *TGF-ß1* and *TGF-ß2*. However, addition of a TGF-β-neutralizing antibody to co-culture did not significantly alter branching as the temporality of TGF-β regulation of branching morphogenesis is likely complex and should be explored further. The most highly expressed gene from qRT-PCR TGF-β profiling arrays was *TGFBI*, an extracellular-matrix-secreted factor recently reported to promote PCa growth and metastasis after androgen deprivation therapy (Chen et al., 2017). This mechanism could be investigated using our co-culture model.

In addition to supporting organized branching morphogenesis, prostate stroma had notable effects on organoid growth and viability. Current culture methods of prostate organoids derived from adult progenitor cells typically yield formation efficiencies <1% (Karthaus et al., 2014) and present a barrier to utilizing human-derived organoids in personalized medicine applications. Under our culture conditions of sparsely seeded epithelial cells, organoids in mono-culture had a formation efficiency ~10%, which increased to >20% with the addition of stroma. Notably, organoid culture using our media and conditions had relatively high formation efficiencies despite containing few added supplements and lacking the ROCK inhibitor, in stark contrast to other specialized conditions with lower efficiencies (Drost et al., 2016). Moreover, employing patient stroma to further enhance the organoid take-rate may mitigate the current limitations of

using patient tissue in *ex vivo* studies and provide an avenue for personalized medicine. Although stromal cells were viable, dividing cells were rare compared with epithelial cell divisions and relieves concerns of stromal overgrowth of the culture.

In our conditions, organoid formation efficiency was further enhanced by reducing the epithelial seeding density to 100 cells/well, which also promoted organoid growth, with organoids >1 mm in diameter and visible with the naked eye. A range of viable prostate organoid culture methods have been reported in the literature (Fang et al., 2013; Härmä et al., 2010; Iacopino et al., 2012), but the phenotypic consequences of cell seeding density have not been described. Differences in organoid size due to seeding density demonstrate that subtle alterations to culture conditions can alter organoid growth phenotypes and should be carefully controlled in experiments.

The generation of cancer organoids or "tumoroids" from localized cancer is a current limitation in the field, as primary human epithelial prostate cells isolated from cancer regions of tissue (PrECa) do not display cancer phenotypes (Peehl, 2004). Recently it was shown that tumoroids derived from PCa metastases and circulating tumor cells retain *in vivo* genomic alterations and morphology when grown *in vitro* and as patient-derived xenografts (Gao et al., 2014). To emphasize how this model may improve the generation of tumoroids in the future, we applied our co-culture model to PrE cells derived from localized cancer regions. Although genomic characterization of our organoids derived from cancer regions was not completed, there was a distinct preservation of AMACR expression that matched the patient cancer tissue and was only seen when organoids were co-cultured with stroma. Additionally, organoids derived from cancer regions were able to retain *AMACR* expression through two passages and further studies should assess AMACR retention in long-term co-culture. Together these findings highlight a promising future direction for tumoroid co-culture that could be pursued both for improved tumoroid viability and as an experimental tool.

Overall, we show that direct contact with prostate stroma induces organoid branching reminiscent of nascent epithelial morphogenesis and better recapitulates tissue structure. Incorporation of prostate stroma is essential to accurately model both the prostate and PCa disease *in vitro* and provides the field with a valuable culture model for studying stromal-epithelial cross talk in development and disease.

Limitations of the Study

There are a few limitations to consider pertaining to this study, particularly in regard to the low number of passages used to explore the maintenance of *AMACR* expression (Figures 5C and S5). As mentioned in the discussion, future studies may focus on the number of passages for which the organoids derived from cancer regions can be maintained. Full genomic, transcriptomic, and phenotypic validation of the cancer organoids is also warranted.

METHODS

All methods can be found in the accompanying Transparent Methods supplemental file.

SUPPLEMENTAL INFORMATION

Supplemental Information includes Transparent Methods, 6 figures, and 10 videos and can be found with this article online at https://doi.org/10.1016/j.isci.2019.01.028.

ACKNOWLEDGMENTS

We thank the UIC Biorespository members, Dr. Klara Valyi-Nagy and Alex Susma, and the urologists, Drs. Michael Abern, Daniel Moreira, and Simone Crivallero, for facilitation of the tissue acquisition for the primary cell cultures. We thank the UIC Urology patients for donating their tissue to research. We thank Ke Ma at the UIC Fluorescence Imaging Core for assisting with confocal. We thank Manny Alonso and Maria Sverdlov at the UIC Histology and Tissue Imaging Core for assisting with AMACR staining. We thank Julian Pachecho for his help with Celleste™ analysis. This work was funded, in part, by the Department of Defense Prostate Cancer Research Program Health Disparities Idea Award PC121923 (Nonn) and the UIC Center for Clinical and Translation Science Pre-doctoral Education for Clinical and Translational Scientists (PECTS) Program (Richards, McCray) and by the National Institutes of Health's National Cancer Institute, grant numbers U54CA202995, U54CA202997, and U54CA203000, known as the Chicago Health Equity

Collaborative (L.N., A.B.M., M.M., C.V., and S.A.A.). The content is solely the responsibility of the authors and does not necessarily represent the official views of the National Institutes of Health or the Department of Defense.

AUTHOR CONTRIBUTIONS

Conceptualization, Z.R., G.S.P., S.A.A., and L.N.; Methodology, Z.R., J.M., and T.M.; Investigation, Z.R., J.M., T.M., J.T.M., J.G., and M.L.Z.; Resources, L.N.; Writing – original draft, Z.R. and L.N.; Writing – Review and editing, T.M., Z.R., L.N., C.V., S.A.A., G.S.P., A.B.M.; Visualization, Z.R., and J.M.; Supervision, L.N., G.S.P., C.V., A.B.M., S.A.A.; Funding acquisition, L.N., C.V., S.A.A., A.B.M, M.M.

DECLARATION OF INTERESTS

The authors declare no competing interests.

Received: March 2, 2018
Revised: June 6, 2018
Accepted: January 18, 2019
Published: February 22, 2019

SUPPORTING CITATIONS

The following reference appears in the Supplemental Information: Livak and Schmittgen, 2001.

REFERENCES

Åkerfelt, M., Bayramoglu, N., Robinson, S., Toriseva, M., Schukov, H.-P., Härmä, V., Virtanen, J., Sormunen, R., Kaakinen, M., Kannala, J., et al. (2015). Automated tracking of tumor-stroma morphology in microtissues identifies functional targets within the tumor microenvironment for therapeutic intervention. Oncotarget *6*, 30035–30056.

Ananthanarayanan, V., Deaton, R.J., Yang, X.J., Pins, M.R., and Gann, P.H. (2005). Alpha-methylacyl-CoA racemase (AMACR) expression in normal prostatic glands and high-grade prostatic intraepithelial neoplasia (HGPIN): association with diagnosis of prostate cancer. Prostate *63*, 341–346.

Barron, D.A., and Rowley, D.R. (2012). The reactive stroma microenvironment and prostate cancer progression. Endocr. Relat. Cancer *19*, R187–R204.

Chen, W.-Y., Tsai, Y.-C., Yeh, H.-L., Suau, F., Jiang, K.-C., Shao, A.-N., Huang, J., and Liu, Y.-N. (2017). Loss of SPDEF and gain of TGFBI activity after androgen deprivation therapy promote EMT and bone metastasis of prostate cancer. Sci. Signal. *10*, 1–10.

Chua, C.W., Shibata, M., Lei, M., Toivanen, R., Barlow, L.J., Bergren, S.K., Badani, K.K., McKiernan, J.M., Benson, M.C., Hibshoosh, H., et al. (2014). Single luminal epithelial progenitors can generate prostate organoids in culture. Nat. Cell Biol. *16*, 951–961.

Cunha, G.R., and Chung, L.W.K. (1981). Stromal-epithelial interactions—I. Induction of prostatic phenotype in urothelium of testicular feminized (Tfm/y) mice. J. Steroid Biochem. *14*, 1317–1324.

Drost, J., Karthaus, W.R., Gao, D., Driehuis, E., Sawyers, C.L., Chen, Y., and Clevers, H. (2016). Organoid culture systems for prostate epithelial and cancer tissue. Nat. Protoc. *11*, 347–358.

Fang, X., Sittadjody, S., Gyabaah, K., Opara, E.C., and Balaji, K.C. (2013). Novel 3D co-culture model for epithelial-stromal cells interaction in prostate cancer. PLoS One *8*, e75187.

Farnsworth, W.E. (1999). Prostate stroma: physiology. Prostate *38*, 60–72.

Franco, O.E., Shaw, A.K., Strand, D.W., and Hayward, S.W. (2010). Cancer associated fibroblasts in cancer pathogenesis. Semin. Cell Dev. Biol. *21*, 33–39.

Franco, O.E., Jiang, M., Strand, D.W., Peacock, J., Fernandez, S., Jackson, R.S., Revelo, M.P., Bhowmick, N.A., and Hayward, S.W. (2011). Altered TGF-β signaling in a subpopulation of human stromal cells promotes prostatic carcinogenesis. Cancer Res. *71*, 1272–1281.

Gao, D., Vela, I., Sboner, A., Iaquinta, P.J.J., Karthaus, W.R.R., Gopalan, A., Dowling, C., Wanjala, J.N.N., Undvall, E.A.A., Arora, V.K.K., et al. (2014). Organoid cultures derived from patients with advanced prostate cancer. Cell *159*, 176–187.

Garraway, I.P., Sun, W., Tran, C.P., Perner, S., Zhang, B., Goldstein, A.S., Hahm, S.A., Haider, M., Head, C.S., Reiter, R.E., et al. (2010). Human prostate sphere-forming cells represent a subset of basal epithelial cells capable of glandular regeneration in vivo. Prostate *70*, 491–501.

Giangreco, A.A., Vaishnav, A., Wagner, D., Finelli, A., Fleshner, N., Van der Kwast, T., Vieth, R., and Nonn, L. (2013). Tumor suppressor microRNAs, miR-100 and -125b, are regulated by 1,25-dihydroxyvitamin D in primary prostate cells and in patient tissue. Cancer Prev. Res. (Phila.) *6*, 483–494.

Giangreco, A.A., Dambal, S., Wagner, D., Van der Kwast, T., Vieth, R., Prins, G.S., and Nonn, L. (2015). Differential expression and regulation of vitamin D hydroxylases and inflammatory genes in prostate stroma and epithelium by 1,25-dihydroxyvitamin D in men with prostate cancer and an in vitro model. J. Steroid Biochem. Mol. Biol. *148*, 156–165.

Gjorevski, N., Sachs, N., Manfrin, A., Giger, S., Bragina, M.E., Ordóñez-Morán, P., Clevers, H., and Lutolf, M.P. (2016). Designer matrices for intestinal stem cell and organoid culture. Nature *539*, 560–564.

Hannezo, E., Scheele, C.L.G.J., Moad, M., Drogo, N., Heer, R., Sampogna, R.V., van Rheenen, J., and Simons, B.D. (2017). A unifying theory of branching morphogenesis. Cell *171*, 242–255.e27.

Härmä, V., Virtanen, J., Mäkelä, R., Happonen, A., Mpindi, J.P., Knuuttila, M., Kohonen, P., Lötjönen, J., Kallioniemi, O., and Nees, M. (2010). A comprehensive panel of three-dimensional models for studies of prostate cancer growth, invasion and drug responses. PLoS One *5*, e10431.

Hayward, S.W., Rosen, M.A., and Cunha, G.R. (1997). Stromal-epithelial interactions in the normal and neoplastic prostate. Br. J. Urol. *79* (*Suppl 2*), 18–26.

Iacopino, F., Angelucci, C., and Sica, G. (2012). Interactions between normal human fibroblasts and human prostate cancer cells in a co-culture system. Anticancer Res. *32*, 1579–1588.

Jiang, Z., Woda, B.A., Wu, C.-L., and Yang, X.J. (2004). Discovery and clinical application of a novel prostate cancer marker: alpha-methylacyl CoA racemase (P504S). Am. J. Clin. Pathol. *122*, 275–289.

Karthaus, W.R., Iaquinta, P.J., Drost, J., Gracanin, A., van Boxtel, R., Wongvipat, J., Dowling, C.M., Gao, D., Begthel, H., Sachs, N., et al. (2014). Identification of multipotent luminal progenitor

cells in human prostate organoid cultures. Cell *159*, 163–175.

Kretzschmar, K., and Clevers, H. (2016). Organoids: modeling development and the stem cell Niche in a dish. Dev. Cell *38*, 590–600.

Lang, S.H., Stark, M., Collins, A., Paul, A.B., Stower, M.J., and Maitland, N.J. (2001). Experimental prostate epithelial morphogenesis in response to stroma and three-dimensional matrigel culture. Cell Growth Differ. *12*, 631–640.

Liao, C.-P.C.-P., Adisetiyo, H., Liang, M., and Roy-Burman, P. (2010). Cancer-associated fibroblasts enhance the gland-forming capability of prostate cancer stem cells. Cancer Res. *70*, 7294–7303.

Livak, K.J., and Schmittgen, T.D. (2001). Analysis of relative gene expression data using real-time quantitative PCR and the 2−ΔΔCT method. Methods *25*, 402–408.

Niu, Y.-N., and Xia, S.-J. (2009). Stroma-epithelium crosstalk in prostate cancer. Asian J. Androl. *11*, 28–35.

Nonn, L., Peng, L., Feldman, D., and Peehl, D.M. (2006). Inhibition of p38 by vitamin D reduces interleukin-6 production in normal prostate cells via mitogen-activated protein kinase phosphatase 5: implications for prostate cancer prevention by vitamin D. Cancer Res. *66*, 4516–4524.

Peehl, D.M. (2004). Are primary cultures realistic models of prostate cancer? J. Cell. Biochem. *91*, 185–195.

Prins, G.S., and Putz, O. (2008). Molecular signaling pathways that regulate prostate gland development. Differentiation *76*, 641–659.

Rubin, M.A., Zhou, M., Dhanasekaran, S.M., Varambally, S., Barrette, T.R., Sanda, M.G., Pienta, K.J., Ghosh, D., and Chinnaiyan, A.M. (2002). alpha-Methylacyl coenzyme A racemase as a tissue biomarker for prostate cancer. JAMA *287*, 1662–1670.

Sasaki, T., Franco, O.E., and Hayward, S.W. (2017). Interaction of prostate carcinoma-associated fibroblasts with human epithelial cell lines in vivo. Differentiation *96*, 40–48.

Silberstein, G.B., and Daniel, C.W. (1987). Reversible inhibition of mammary gland growth by transforming growth factor-beta. Science *237*, 291–293.

Wang, S., Gao, D., and Chen, Y. (2017). The potential of organoids in urological cancer research. Nat. Rev. Urol. *14*, 401–414.

ISCI, Volume *12*

Supplemental Information

Prostate Stroma Increases the Viability and Maintains the Branching Phenotype of Human Prostate Organoids

Zachary Richards, Tara McCray, Joseph Marsili, Morgan L. Zenner, Jacob T. Manlucu, Jason Garcia, Andre Kajdacsy-Balla, Marcus Murray, Cindy Voisine, Adam B. Murphy, Sarki A. Abdulkadir, Gail S. Prins, and Larisa Nonn

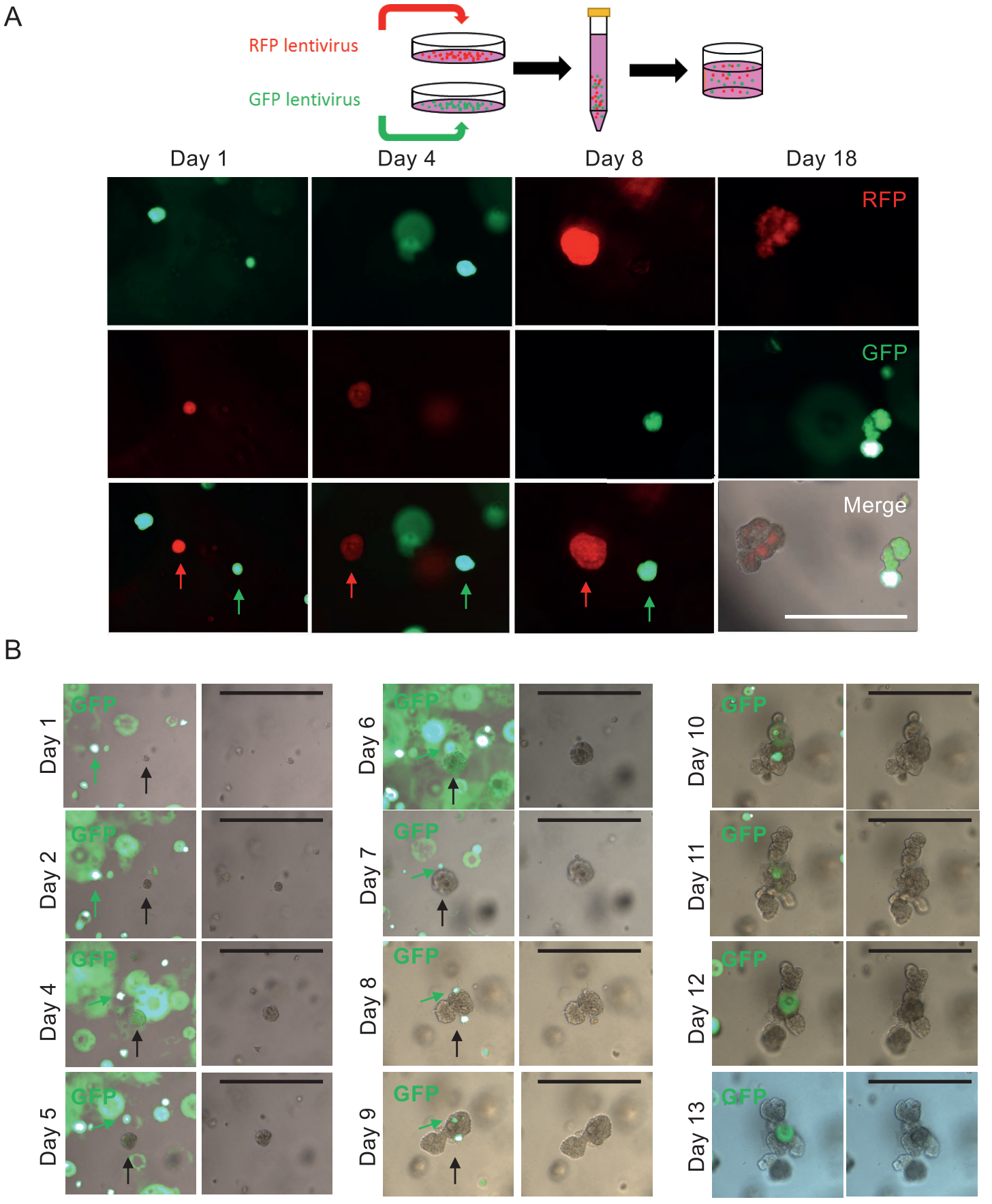

Supplemental Figure 1. Organoids are derived from single cells, related to Figure 1.

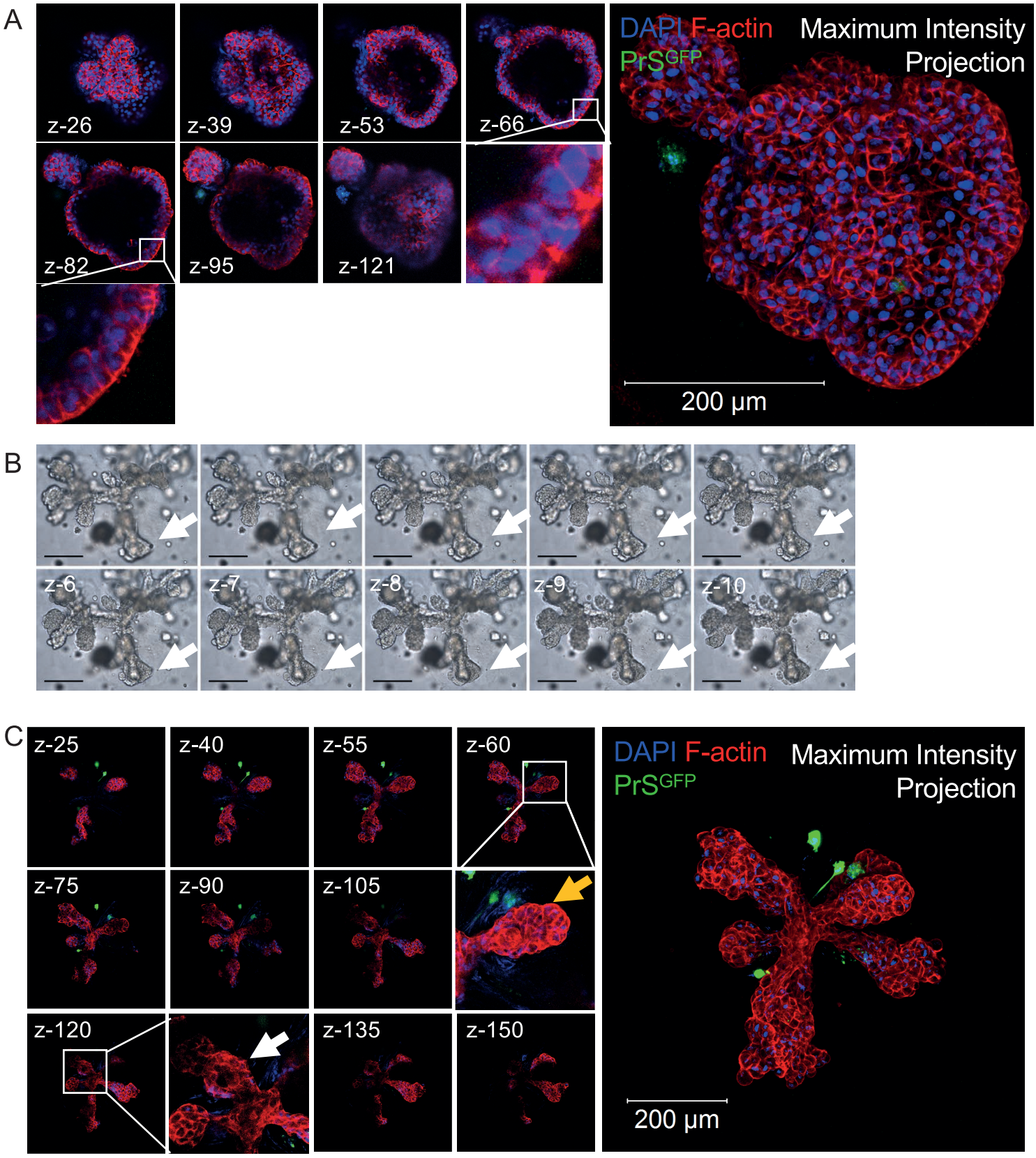

Supplemental Figure 2. Organoids in co-culture contain lumens, related to Figure 2

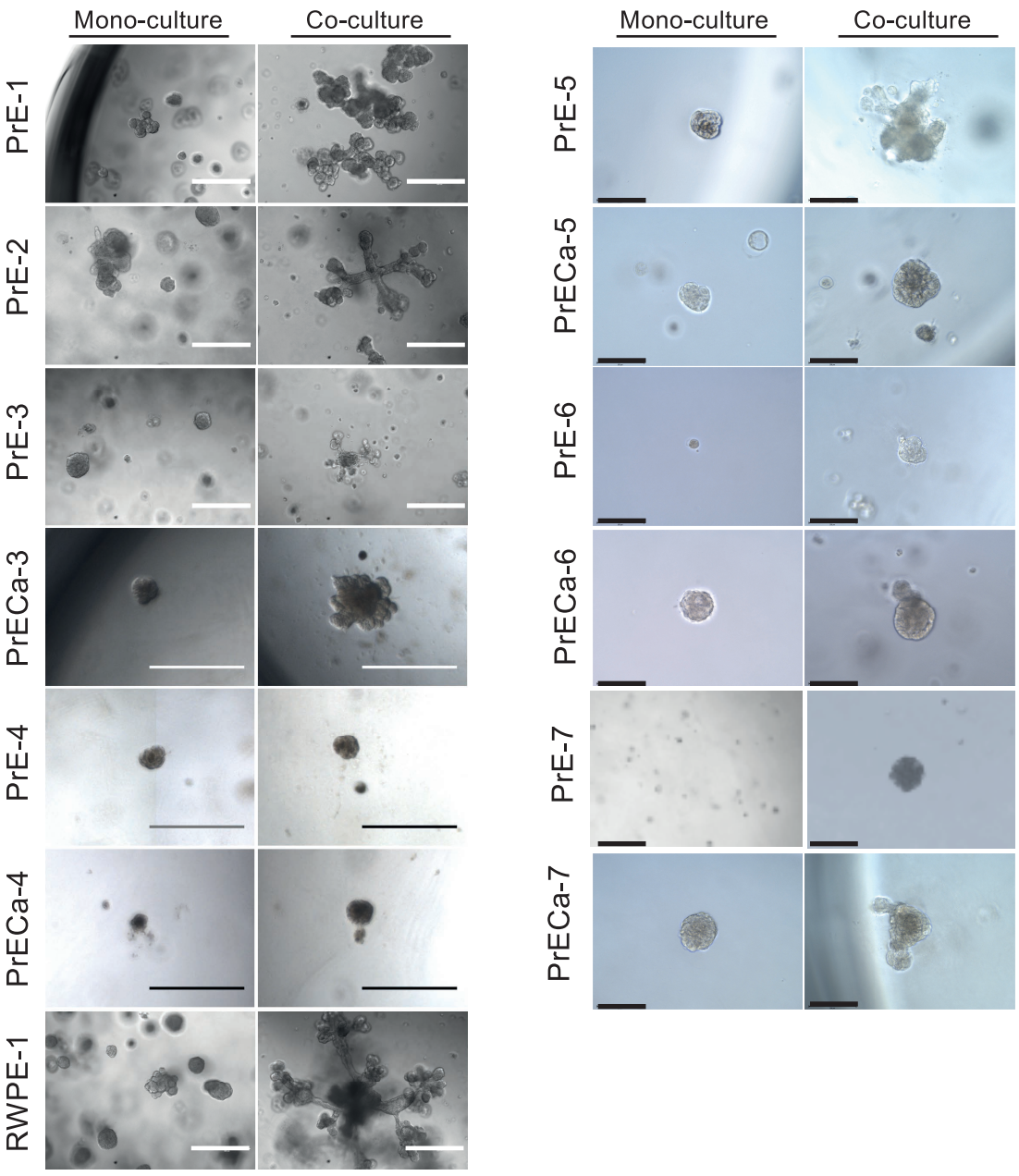

Supplemental Figure 3. Organoids exhibit inter-patient heterogeneity, related to Figure 2 and Table 1

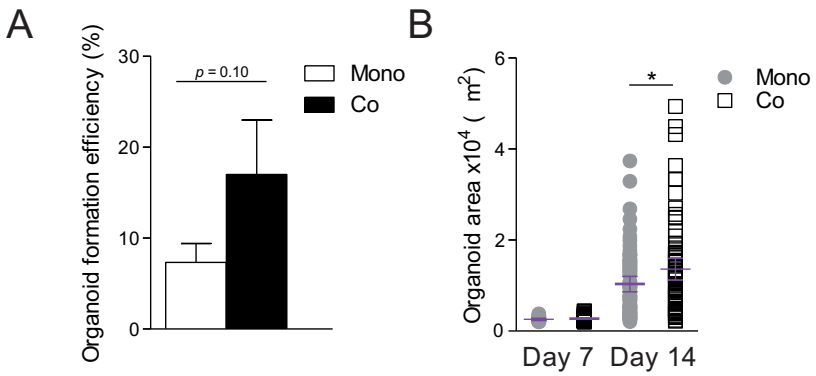

Supplemental Figure 4. Formation efficiency and area of organoids in co-culture with NIH-3T3 fibroblasts, related to Figure 4

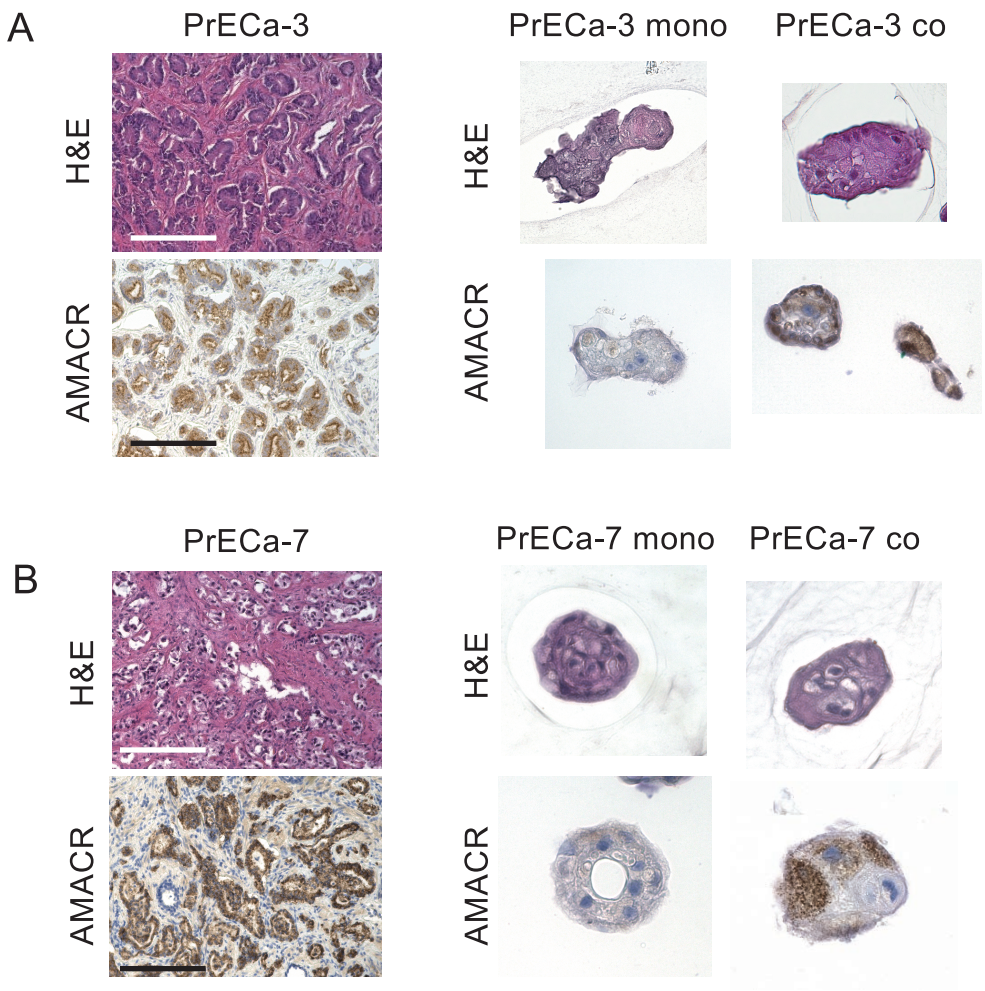

Supplemental Figure 5. Images and AMACR staining in co-cultured organoids derived from cancer regions, related to Figure 5.

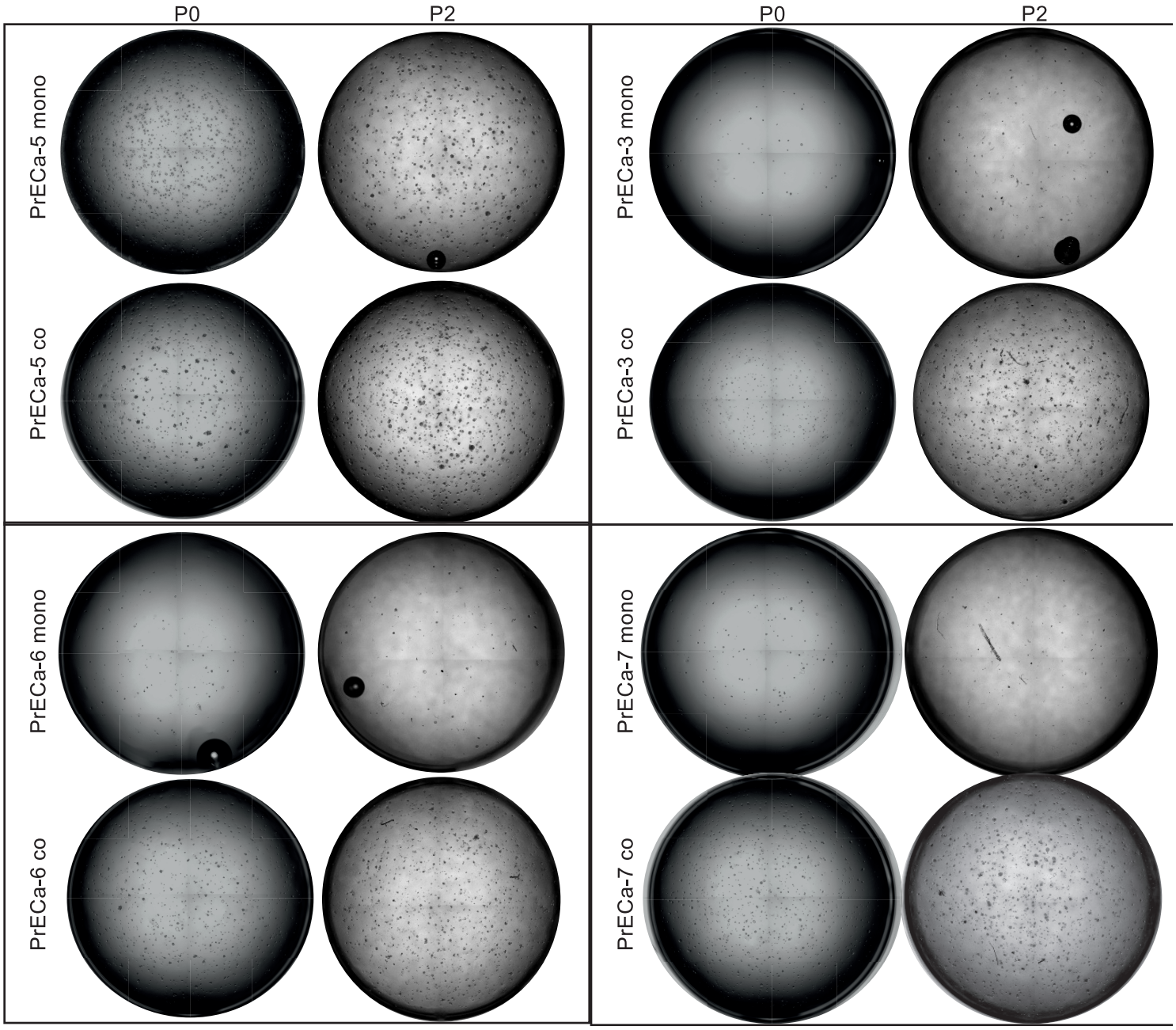

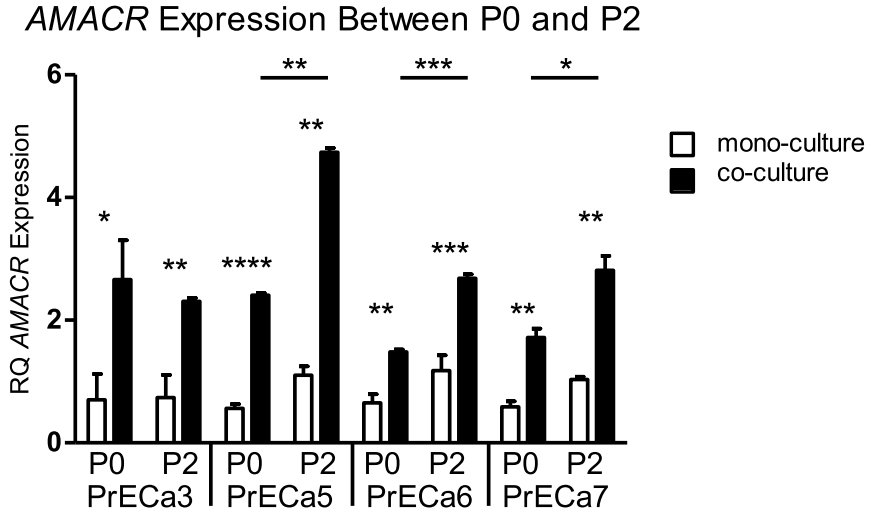

Supplemental Figure 6. Images and *AMACR* expression of co-cultured organoids derived from cancer regions at passage 0 and passage 2, related to Figure 5

Supplemental Video, Data and Excel Table Title and Legends

Video Titles

Movie 1. Organoid at day 7 in co-culture exhibiting branching morphogenesis. Cells used, PrE-1 and PrS mix 1.

Movie 2. Organoid at day 7 in mono-culture exhibiting branching morphogenesis. Cells used, PrE-1.

Movie 3. Stromal cell (right) taxis towards a branching organoid (left) in co-culture. Cells used, PrE-1 and PrS mix 1.

Movie 4. Stromal cell (bottom left) taxis towards an organoid and subsequent influence on organoid budding and branching distal to stroma-organoid contact. Cells used, PrE-1 and PrS mix 1.

Movie 5. Stromal cell pseudopodia extension (bottom right) and direct contact with an organoid. Subsequent bud formation and elongation occurred distal to stroma-organoid contact. Cells used, PrE-1 and PrS mix 1.

Movie 6. Stromal cells (top right) in direct contact and migrating with a branched organoid. Complex stalk elongation occurred distal to stroma-organoid contact. Cells used, PrE-1 and PrS mix 1.

Movie 7. Organoid in co-culture exhibiting complex branching morphogenesis. Bud detachment occurred after 29 hours (top of organoid), and stalk detachment at 31 hours (top of frame). Cells used, PrE-1 and PrS mix 1.

Movie 8. Organoid co-cultured with GFP-labeled PrS cells integrated with more complex organoid structures. Cells used, PrE-1 and PrS mix 3.

Movie 9. PrS cell at day 7 in co-culture exhibiting pseudopodia expansion and contraction, and remodeling of the surrounding matrix. Cells used, PrE-1 and PrS mix 1.

Movie 10. Organoid co-cultured with GFP-labeled mouse embryonic fibroblasts (NIH-3T3 cells). Extensive cell-cell contact and encapsulation of organoids inhibited branching. Cells used, PrE-1.

Movies are composed of time-lapse images taken every 5 minutes. Time format, hour:min.

Supplemental Data Titles and Legends

Supplemental Figure 1. Organoids are derived from single cells, related to Figure 1

(A) PrE-2 cells were separately transduced with a lentivirus RFP or GFP reporter, mixed and plated into 3D culture. Resulting organoids were imaged at day 1, 4, 8, and 18 and show clonal origin of each organoid. Scale bar 500μm.

(B) PrE-1 cells were plated in co-culture with GFP-labeled PrS mix 5, epithelial cells were identified as GFP(-) and their locations were recorded, followed, and imaged over days 0-13 to capture expansion into organoid. Figure shows outgrowth of a single cell to a branched organoid. GFP+ stromal cells (green arrow) are visible throughout, moving around day to day and touching the organoid (black arrow). Scale Bar 500μm.

Supplemental Figure 2. Organoids in co-culture contain lumens, related to Figure 2

(A) Whole-mounted fluorescent z-stack images and maximum intensity projected image (right) of PrE-1 organoid co-cultured with PrS^{GFP}, stained with phalloidin and DAPI; lumen in zoom panels at z-66 and z-82.

(B) Sequential z-stack images of a day 14 organoid grown from PrE-1 cells. White arrow shows a branch containing hollow luminal space. Scale bar 200μm

(C) Whole-mounted fluorescent z-stack images and maximum intensity projected image (right) of PrE-1 organoid co-cultured with PrS^{GFP}, stained with phalloidin and DAPI; showing some solid chords (zoom, z-60 yellow arrow) and branches that contain lumens (zoom, z-120 white arrow).

Supplemental Figure 3. Organoids exhibit inter-patient heterogeneity, related to Figure 2 and Table 1

Brightfield images of organoids from all 12 tissues (7 patients) used and RWPE-1 cells grown in mono- and co-culture 3D conditions. Mono and co-culture images from the same patient were captured on the same day. All images in the left panel were taken between days 7 and 10, co-culture images were grown with PrS mix 1. The right panel were taken on day 13 of culture, co-culture images for PrE-5/PrECa-5 was grown with PrS mix 5, and PrE-6/PrECa-6 and PrE-7/PrECa-7 were grown with PrS mix 5. Scale bars 500μm. See Table 1 for patient characteristics.

Supplemental Figure 4. Formation efficiency and area of organoids in co-culture with NIH-3T3 fibroblasts, related to Figure 4

(A) Formation efficiency of organoids in mono-culture and in co-culture with NIH-3T3 fibroblasts assessed on day 7. Triplicate wells per condition, error bars represent standard error of the mean.

(B) Area quantification of organoids grown in mono-culture and co-culture with NIH-3T3 fibroblasts after 7 and 14 days. Triplicate wells analyzed per condition, error bars show mean with 95% confidence.

Organoids were grown from PrE-1 cells. A p-value <0.1 was considered statistically significant where * = $p < 0.1$, ** = $p < 0.05$, *** = $p < 0.01$, **** = $p < 0.001$ (ns, not signficant).

Supplemental Figure 5. Images and AMACR staining in co-cultured organoids derived from cancer regions, related to Figure 5.

(A) Matched benign (PrE-3) and cancer (PrECa-3) tissue with hematoxylin and eosin staining (left, top panel) and presence of AMACR by immunohistochemistry (left, bottom panel). 10X image shown with 40X inset for AMACR. Organoids with hematoxylin and eosin staining (right, top panel) and AMACR by immunohistochemistry (right, bottom panel).

(B) Matched benign (PrE-7) and cancer (PrECa-7) tissue with hematoxylin and eosin staining (left, top panel) and presence of AMACR by immunohistochemistry (left, bottom panel). 10X image shown with 40X inset for AMACR. Organoids with hematoxylin and eosin staining (right, top panel) and AMACR by immunohistochemistry (right, bottom panel), organoids were not viable for RNA or embedding.

Supplemental Figure 6. Images and *AMACR* expression of co-cultured organoids derived from cancer regions at passage 0 and passage 2, related to Figure 5

(A) Whole-well images of organoids derived from cancer regions were obtained at day 7 on passage 0 (left) and passage 2 (right).

(B) Gene expression of AMACR in passage 0 and passage 2 organoids derived from cancer regions by RT-qPCR. A p-value <0.1 was considered statistically significant where * = $p < 0.1$, ** = $p < 0.05$, *** = $p < 0.01$, **** = $p < 0.001$ (ns, not signficant).

Transparent Methods

CONTACT FOR REAGENT AND RESOURCE SHARING

Further information and requests for resources and reagents should be directed to and will be fulfilled by the Lead Contact, Larisa Nonn (lnonn@uic.edu).

EXPERIMENTAL MODEL AND SUBJECT DETAILS

Primary cell lines
Primary prostate cells established from fresh male radical prostatectomy tissues were isolated as previously described (Giangreco et al., 2013; Nonn et al., 2006). Briefly, radical prostatectomy tissue from benign and cancer regions of the peripheral zone was collected according to UIC Internal Review Board-approved protocol and patients consented prior to surgery. See **Table 1** for primary cell patient characteristics. Tissue histology was confirmed by a board-certified pathologist. Tissue was digested in collagenase/trypsin to single cells and cultured in either Prostate Cell Growth Media (Lonza) or MCDB-105 media (Sigma-Aldrich) to select for epithelial (PrE and PrECa) or stromal cell (PrS) populations, respectively. When ~70% confluent, cells are cryopreserved singly and thawed prior to experimentation. Epithelial population purity was authenticated by expression of the epithelial specific markers *CK5*, *CK8*, *CK18*, and *p63* by RT-qPCR. Stromal cell purity was authenticated by lack of epithelial marker expression and expression of the stroma specific marker *TIMP3*. See Table 1 for patient characteristics.

Cell Lines
NIH-3T3 cells were generously provided by Dr. Alan Diamond, and originally purchased from ATCC. Cells were cultured in Dulbecco's Modified Eagle Medium (DMEM) supplemented with 10% fetal bovine serum (FBS). RWPE-1 cells were purchased from ATCC (2014), frozen in multiple low-passaged aliquots, re-authenticated in 2016, and used only at passages <20. RWPE-1 cells were cultured in Keratinocyte serum free medium (KSFM). All cells cultured at standard 37°C with 5% CO_2.

METHOD DETAILS

3D Organoid Mono- and Co-culture
Epithelial cells were grown at passage 2 from thaw in 100 mm collagen-coated dishes to ~70% confluent. To seed cells singly in 3D mono-cultures, the specified number of epithelial cells were mixed with media containing 33% growth factor reduced phenol red-free Matrigel (Corning). Cultures were grown using a flat-bottom 96-well microplate containing a 50 µL base layer of 50% Matrigel in media. Once the base layer solidified, 100 µL of the cell and Matrigel mixture was plated directly on top of the base layer and allowed to solidify for at least 1 hour at 37ºC. Once solid, 100 µL of keratinocyte serum-free media supplemented with 5% charcoal-stripped fetal bovine serum and 10 nM dihydrotestosterone were added to each well. Cultures were grown for up to 28 days and media replaced every 3 days.

For 3D co-cultures, stromal cells were grown from thaw up to 90% confluent. Epithelial and stromal cells were mixed at specified ratios in keratinocyte serum-free media supplemented with 5% charcoal-stripped fetal bovine serum and 10nM dihydrotestosterone containing 33%

Matrigel. Co-cultures were plated identically to mono-culture described above, with cells seeded singly and free of clumps.

Transwell Insert Co-culture

Primary stromal cells were grown from thaw up to 90% confluent then seeded at 5,000 cells/insert onto 0.4µm Transwell inserts (Corning) one day prior to co-culture. 3D cultures were prepared in 12-well microplates with a 125uL base layer of 50% Matrigel followed by addition of 250 epithelial cells in 250µL of 33% Matrigel per well. The microplate was tilted to promote Matrigel solidification in a crescent shape in the corner of each well for at least one hour at 37ºC. Once solid, Transwell inserts containing the stromal cells were transferred to epithelial containing wells. Epithelial cells were grown from thaw in 100mm collagen-coated dishes up to 70% confluent prior to 3D culture. For direct co-culture controls, 250 PrE cells were mixed with 5,000 PrS cells in 250uL of 33% Matrigel. All Transwell experiments completed in keratinocyte serum-free media supplemented with 5% charcoal-stripped fetal bovine serum and 10nM dihydrotestosterone. Cultures were imaged for analysis after 14 days of co-culture.

Brightfield Image Acquisition, Processing, and Analysis

Images of each culture were acquired at 4x magnification using the Evos FL Auto 2 Imaging System (Thermo Fisher Scientific). A whole-well enhanced depth-of-field image was generated for each well by acquiring up to 25 images in the z-plane in covering four quadrants of each well. Images from each quadrant at every z-position were stitched together and the z-stack compressed to a single enhanced depth-of-field image using Celleste™ Image Analysis Software (Thermo Fisher Scientific).

Organoid count, area, circularity, and maximum/minimum radius ratio metrics were generated by manual and automated assisted identification of each organoid. Image analysis and measurements were performed using Celleste™ Image Analysis Software (Thermo Fisher Scientific).

Immunofluorescence and Immunohistochemistry

PrS mix 3 cells were grown on a glass chamber slide, fixed in 4% paraformaldehyde for 1 hour, and incubated with rabbit polyclonal anti-vimentin (Proteintech Group) and monoclonal anti-smooth muscle actin (M0851)(Dako) antibodies, counterstained with DAPI and imaged on the Vectra3 confocal microscope (PerkinElmer).

Organoids were dissociated in Dispase (1 U/mL, STEMCELL Technologies), resuspended in HistoGel™ (Thermo Fisher Scientific), solidified at 4ºC, fixed in 4% paraformaldehyde for 1 hour, transferred to 70% ethanol, and paraffin-embedded. 5µm sections were incubated with polyclonal guinea pig anti-Cytokeratin 8/18 (03-GP11)(American Research Products, Inc), rabbit monoclonal anti-p63a antibody (D2K8X)(Cell Signaling Technology), counterstained with DAPI and imaged on the Vectra3 confocal microscope.

Formalin-fixed and paraffin embedded organoid sections of 5µm were also incubated with monoclonal rabbit anti-androgen receptor antibody (D6F11)(Cell Signaling Technology), 3,3'-Diaminobenzidine for visualization, and counterstained with hematoxylin immunohistochemical staining.

For whole mount immunofluorescence, organoids were transferred by pipette to a chamber slide (Nunc Lab-Tek II Chamber Slide System) and fixed in 4% paraformalydehyde. GFP fluorescence from GFP-labeled PrS cells was quenched with 50mM NH_4Cl (Fig 2C), quenching step was skipped for PrS-GFP whole mount observation (Fig2D, Fig S3). Fixed organoids were

permeabilized and incubated in polyclonal guinea pig anti-Cytokeratin 8/18 (03-GP11)(American Research Products, Inc), polyclonal rabbit anti-Keratin 5 (905501)(BioLegend), counterstained with Alexa Fluor™ 647 Phalloidin (Thermo Fisher Scientific) and DAPI, and imaged on the Zeiss LSM 710 confocal microscope.

Radical prostatectomy tissue sections of 5 µm and formalin-fixed and paraffin embedded organoid sections of 5µm were incubated with mouse monoclonal anti-AMACR antibody (13H4)(Genemed) and counterstained with hematoxylin for immunohistochemical staining.

Lentivirus Transduction

NIH-3T3 and PrS cells were transduced with pGreenPuro Scramble Hairpin lentivirus (System Biosciences) and selected by passaging at least once into media containing 1-3 µg/mL puromycin until all cells were GFP+. Cells at lowest passage were cryofrozen and thawed before use.

For determination of single cell origin of organoids, PrE-2 cells were transduced with lentiviral vectors for GFP (MZIP000-VA-1)(System Biosciences) at an MOI of 20 or RFP (LVP309)(GenTarget Inc.) at an MOI of 6.25 with puromycin resistance. Cells were selected with puromycin treatment for at least 1 passage, mixed, and seeded into 3D culture as described. Organoids were imaged after 18 days of culture using the Evos FL Auto 2 Imaging System.

Tissue Histology

Tissue from each patient isolated for primary cell culture was also used for histopathology. Briefly, a small piece was collected, formalin-fixed, and paraffin-embedded. Sections of 5 µm were obtained and stained with hematoxylin and eosin for pathological assessment.

Proliferation assay

Stromal cells grown in 3D mono-culture for 4 days were incubated with Click-iT™ EdU (Thermo Fisher Scientific) for 48 hours. Matrigel was dissociated with Dispase (1 U/mL) and cells visualized for EdU fluorescence and DAPI counterstain.

Organoids co-cultured with GFP-labeled PrS cells were incubated with Click-iT™ EdU (Thermo Fisher Scientific) for 24 hours. Whole organoids and associated stromal cells were collected by pipette and transferred to a chamber slide (Nunc Lab-Tek II Chamber Slide System). Cells were fixed in 3.7% formaldehyde and visualized for EdU fluorescence and Hoechst counterstain using the Zeiss LSM 710 confocal microscope.

The number of PrS cells after 7 of 3D culture was quantified by dissociating the Matrigel with Dispase (1 U/mL) and counted using a hemocytometer.

PCR Profiling Arrays and RT-qPCR gene expression

Stromal cells were grown to 90% confluent in 2D prior to seeding in 3D. A total 10,000 cells/well were plated in mono-culture conditions as described above. Matrigel in the 3D cultures was dissociated with Dispase (1 U/mL), washed with HBS, and collected in Trizol (Thermo Fisher Scientific). RNA was isolated using the Trizol extraction method, and RNA quantity and quality determined by NanoDrop Spectrophotometer (Thermo Fisher Scientific). cDNA was generated with Qiagen RT^2 First Strand Kit (Qiagen) and gene expression assessed using the Human Growth Factors and Human TGFß/BMP Signaling Pathway Plus RT^2 Profiler PCR Arrays (Qiagen). Arrays were run on a QuantStudio6 (Thermo Fisher Scientific) and normalized

independently using 5 reference genes according to the manufacture's protocol. The $\Delta\Delta C_T$ method was used for comparative analysis (Livak and Schmittgen, 2001).

Matched benign-cancer cells grown in 2D, 3D and 3D co-culture were harvested for RNA using the Trizol method described above. 500 ng of RNA was reverse transcribed using SuperScript™ IV First-Strand Synthesis System (Thermo Fisher Scientific) and qPCR performed on the QuantStudio6 machine. Reference genes *GAPDH* with forward primer 5'-AAGGTCGGAGTCAACGGATTTGGT-3' and reverse 5'-TGATGACAAGCTTCCCGTTCTCAG-3', *KRT5* with forward primer 5'- ATCGCCACTTACCGCAAGC-3' and reverse 5'-CCATATCCAGAGGAAACACTGC-3', *KRT8* with forward primer 5'-GCTGGTGGAGGACTTCAAGA-3' and reverse 5'- TCGTTCTCCATCTCTGTACGC-3', and *CDH1* forward primer 5'-ATGAGTGTCCCCCGGTATCT-3' and reverse 5'-GGTCAGTATCAGCCGCTTTC-3' were used for normalization. Expression of *AMACR* was quantified using forward primer 5'-GTGCTGCTGGAGCCCTTC-3' and reverse primer 5'-CAGCTGGAGTTTCTCCATGA-3' and normalized to the reference gene *GAPDH* (Fig S5A PrE3-PrECa-3, PrE4-PrECa-4) or mean *KRT5, KRT8, CDH1* (Fig 5 D, Fig S5A PrE6-PrECa-6, PrE7PrECa-7). Presence of a TMPRSS2 fusion gene was tested using *TMPRSS2* forward primer 5'- TAGGCGCGAGCTAAGCAGGAG-3' in combination with reverse primers 5'-CCGCACATGGTCTGTACTCCA TA-3' or 5'- CCGTGGAGAGTTTTGTAAGGC T-3' for *ERG*, or reverse primer 5'- TCCCGATACATTCCTGGCTC-3' for *ETV1*.

Organoid Passaging

Organoids were harvested every 5-7 days in Dispase (1U/mL) to dissociate Matrigel and incubated in TrypLE™ Express Enzyme (Gibco) for single cell suspension. Single cells were re-plated in 33% matrigel over a 50% baselayer. Co-cultures were spiked with 1k additional stromal cells per well to account for cell loss during passaging. Media was supplemented overnight with 25 µ Rho-kinase inhibitor (Y-27632, STEMCELL) and replaced with fresh media the next day.

3D Co-culture Branching Inhibitor Assay

3D mono- and co-cultures were setup as described above and grown for 7 days prior to treatment with 2µg/mL of recombinant human Noggin (R&D Systems), 250nM FGFR inhibitor NVP-BGJ398 (Selleckchem), or monoclonal TGF beta-1,2,3 neutralizing antibody (1D11)(Thermo Fisher Scientific). Media was changed every 2-3 days with freshly prepared treatments and cultures imaged as previously described on day 14 after 7 days of treatment.

QUANTIFICATION AND STATISTICAL ANALYSIS

Statistical analyses were performed with GraphPad Prism version 5 (GraphPad Software). Parameters and experimental details can be found in the figure legends. A two-sided unpaired t-test was used for mono- and co-culture comparisons of organoid formation efficiency, area, circularity, and maximum/minimum radius ratio, and RT-qPCR gene expression. One-way analysis of variance (ANOVA) across mono-culture and co-culture conditions was used for formation efficiency and area. The post-test for linear trend between means is reported when significance threshold was surpassed. Microarray results, heatmaps, and Wikipathways analyses were generated and analyzed using Transcriptome Analysis Console (TAC) Software (Thermo Fisher Scientific). Filtering criteria for differentially expressed genes were > 2 or < -2

fold-change and $p < 0.05$. For Wikipathways analysis the p-value was established using a Fisher's Exact Test from a contingency table of the number of overlapping genes, number of non-overlapping genes, number of genes filtered, and number of genes outside of filter criteria for each pathway. A p-value <0.1 was considered statistically significant where * = $p < 0.1$, ** = $p < 0.05$, *** = $p < 0.01$, **** = $p < 0.001$ (ns, not signficant).

DATA AND SOFTWARE AVAILABILITY

The microarray data discussed in this publication have been deposited in NCBI's Gene Expression Omnibus (GEO) and are accessible through GEO Series accession number GSE115052.